

DELFT UNIVERSITY OF TECHNOLOGY

MASTER THESIS

EE5010

---

Quantifying the dynamic interactions between  
physiological signals to predict the exposure from  
chemicals

---

*Author:*

Sarthak Agarwal (5074959)

*Thesis Committee:*

Dr. Richard Hendriks (TU Delft)

Dr. Carolina Varon (TU Delft)

Dr. Tiago Costa (TU Delft)

Dr. Anne Marie Brouwer (TNO)

Jan Ubbo van Baardewijk (TNO)

*Defense Date:*

August 24, 2021





## Acknowledgement

This thesis is the closing chapter of a long journey through the science of signal processing, data science and mathematics that was only possible with help of many people.

I want to thank my university supervisors Dr Richard Hendriks and Dr Carolina Varon for their consistent support and guidance during my thesis. Your supervision helped me immensely in improving my critical reasoning and research skills. Simulating the algorithms on “Micky-mouse” examples before proceeding to actual implementation is one of the key strategies that I will incorporate into my future projects. I also thank Carolina for her detailed comments and suggestions that helped me in improving my report.

Next, I would like to thank my team, at TNO Soesterberg and Rijswijk. First, I would like to thank Dr Anne Marie and Jan Ubbo van Baardewijk for accepting me in your project as an intern and then for this thesis. Thank you for trusting me, giving me freedom and always being available to help. Jan Ubbo, thank you for your patient and endless hour spent in understanding my approaches and helping me to improve them. Your curiosity inspired me to work hard and be motivated throughout the period. You were not just a supervisor but also a friend, I cherished talking with you regarding the King of the Netherlands, dutch food, culture, Olympics and many more. Secondly, I would like to thank Alex Cornelissen for patiently explaining the datasets and always listening to me about deep mathematics with interest. I enjoyed the lab visit at TNO Rijswijk given by you and Dr Jiska Kentrop.

Next, I would like to thank my friends in the Netherlands who inspired me to work hard, made me feel like part of their family. Without their constant help and support, I won't be able to finish my masters.

Finally, I would thank my parents, brother and sister-in-law for trusting, supporting and always being there for me, sharing my happiness and sorrow. My master degree and thesis are dedicated to my brother without whose sacrifices and support this endeavour was not possible.



## Abstract

Causal inference is a familiar topic in biomedical research and a key concept in the study of connectivity in various physiological systems. This work aimed to analyse the coupling between the beat to beat parameters derived from ECG and respiration. It was the first time such an analysis was carried out in the context of finding the differences caused by chemical's exposure.

We used conditional Granger causality, a popular method to evaluate direct causal relationships. We have incorporated the cardinality constraint in the optimization function of Granger causality (GC) to deal with the high dimensionality challenge. Further, we extended the original formulation GC to evaluate the coupling between two unequally sampled signals. Finally, end to end implementation of the machine learning prediction model using causal features is well illustrated.

We found a consistent decrease in the average coupling strength of breathing parameters after the exposure. But in the case of ECG interactions, no noticeable change was observed. Surprisingly we found no significant links between the ECG and breathing parameters. The support vector machine (SVM) and random forest trained on coupling values differentiate between healthy and exposure samples. The accuracy of trained SVM and random forest on the independent test set were 78% and 75%, respectively.



# Contents

<b>1</b>	<b>Introduction</b>	<b>7</b>
1.1	Problem Statement	7
1.2	Concept of Causality	7
1.3	Simple Examples	10
1.3.1	Two independent Process	11
1.3.2	Two Linearly Coupled Signals	11
1.3.3	Two Non-Linearly Coupled Signals	11
1.4	Contribution	11
1.5	Overview	11
<b>2</b>	<b>Granger Causality: Algorithms and Simulations</b>	<b>13</b>
2.1	Granger Causality estimation	13
2.1.1	Mathematical Formulation	13
2.1.2	Calculation Granger Causality in unequal sampled signals	14
2.1.3	Model Order Selection	16
2.1.4	Solving Regression Equation	17
2.2	Statistical analysis	19
2.2.1	F test	19
2.2.2	Surrogate Analysis	20
2.3	Simulation Results	23
2.3.1	Three Variable Case	23
2.3.2	Eleven Variable Case	25
2.3.3	Equal and Unequal Sampled Granger Causality	27
<b>3</b>	<b>Methodology of Evaluating Coupling in Real Data</b>	<b>30</b>
3.1	Dataset	30
3.2	Preprocessing	31
3.3	Signal Segmentation	32
3.4	Experiment Design	34
<b>4</b>	<b>Classification of Granger Causality for exposure detection</b>	<b>36</b>
4.1	Train Test Stratified Splitting	36
4.2	Features Scaling	38
4.3	Principal Component Analysis	39
4.4	Model Selection	40
4.5	Feature Selection	42
4.6	Implemented Models	44
4.6.1	Random Forest	44
4.6.2	Support Vector Machine	45
<b>5</b>	<b>Result</b>	<b>47</b>
5.1	Interactions Analysis	47
5.1.1	Weighted Graph Density	47
5.1.2	Interactions Insights	48
5.2	Classification Results	52
5.2.1	Evaluation Metrics	52
5.3	Classification Results	54
<b>6</b>	<b>Conclusion</b>	<b>57</b>
6.1	Future Work	57
6.2	Conclusion	58

---

# 1 Introduction

## 1.1 Problem Statement

Workers employed in chemical industries, soldiers serving in war zone areas, farmers using pesticides in their fields, and even medical practitioners treating the patients have a high risk of getting exposure to toxic chemicals. Early detection of the harmful chemical can help doctors to treat the victims effectively [12]. Real-time physiological signals such as breathing, ECG and EEG can be recorded to check their overall health. The different types of intoxication can have distinct effects on the physiological behaviour of the human body. Establishing unique profiles concerning the variety of intoxication will reduce the treatment time and make the cure much more accurate. Further, such unique profiles can aid in developing detailed therapy or medicine to counter the effect of intoxication.

Even though certain aspects of physiological changes can overlap between different agents and exposure routes, each of these combinations is expected to have a unique profile, when looking at the whole of the physiological changes combined. If such profiles can be established, these could be used to reduce the treatment delay, by providing an accurate diagnosis in an early stage of the intoxication. Smart wearable sensors provide an excellent platform to provide real-time data on various measures of physiology, to be trained to recognize intoxication profiles. The current project aims to establish the distinct physiological profiles concerning the type of intoxication and subsequently develop a detection model that differentiates among the different chemical exposures.

To achieve the above goal, we cannot expose humans to Fentanyl and VX chemicals for data collection. We got the data of Guinea pigs that are exposed to previously mentioned chemicals with varying dosages. The ultimate goal of the project is to devise a prediction model that can translate to humans without explicitly collecting their exposure data. In the past, we used the physiological parameters that were derived from ECG, EEG and respiration signals to develop the prediction model [61]. Although, the accuracy of the model was more than 95%, there is no guarantee that the model will generalise well on the human dataset also. Because human physiological signals are influenced by external factors such as motion, mental activities that are varying a lot. We think that the model based on interaction features (or causal relationships) between the physiological parameters might be robust to external factors and so, there is a high chance that the causal algorithm will generalise well among different subjects. This is indeed another aim of the assignment that is left for the future work.

In the past, the coupling analysis in complex cardio-respiratory and cardiovascular systems have shown interesting interactions insights between healthy and diseased persons [42][38][59]. Further, we are interested to see if the causal features are able to differentiate between the different exposure types without considering EEG, which is already proved to be useful [61] but difficult to collect in real-time. Further, causal based approaches will aid in transfer learning [55]. The two most important objectives of this thesis are

- Quantify the interactions between the parameters derived from physiological signals.
- Use the interactions to differentiate between the conditions.

## 1.2 Concept of Causality

Interactions between two signals denote how well the signals are related to each other. That is, whether the knowledge of one signal can help in reducing the uncertainty of another signal. There are two types of interactions or coupling measures, directional and non-directional. Directional coupling explains the strength and direction of the relationship between the signals. Here we investigate the cause and effect. Whereas non-directional only expresses the strength of the link between the two signals. Two popular measures for non-directional coupling are correlation and mutual information.

The famous phrase “correlation does not imply causation” indicates the inability of the correlation measure to conclude about the cause and effect between two variables. A correlation between two variables (X and Y) could be due to following scenarios (more possibilities are possible):

- X is causing Y
- Y is causing X
- X is causing Y and Y is causing X

- X and Y are caused by common variable Z, but X and Y do not cause each other
- X and Y are causing Z, but X and Y do not cause each other
- X is causing Z and Z is causing Y, but X and Y do not cause each other

All the above possibilities are depicted in the Figure 1. Because of several possibilities of the same correlation value, it cannot detect the cause and effect between the two variables.

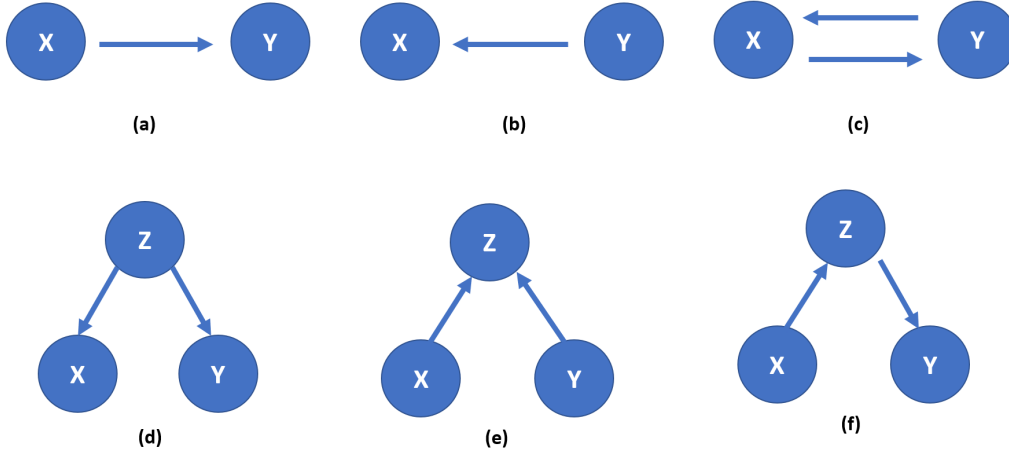


Figure 1: "Correlation does not imply Causation". Different possible scenarios for the non-zero correlation between X and Y. The direction of the arrow indicates the direction of causal relationship. (a) X is causing Y (b) Y is causing X (c) Both X and Y cause each other (d) X and Y are caused by common variable Z, but X and Y do not cause each other (e) X and Y are causing Z, but X and Y do not cause each other (f) X is causing Z and Z is causing Y, but X and Y do not cause each other.

We can compute the correlation using parametric and non-parametric ways. Pearson correlation is a parametric way of measuring the linear correlation between two variables. It is a ratio of the covariance matrix of two variables (X and Y) and the product of their standard deviation. It is denoted as

$$\rho_{xy} = \frac{\Sigma(X, Y)}{\sigma_x \sigma_y} , \text{Lag}=0 \text{ correlation.} \quad (1)$$

The covariance matrix is symmetrical, therefore the mathematical formulation of  $\rho_{xy}$  and  $\rho_{yx}$  are the same. This implies that, if we calculate the correlation for  $x \rightarrow y$  and  $y \rightarrow x$  both will be same. Another method to calculate correlation is a spearman correlation [65]. It is a non-parametric way of measurement that ranks the variables' points in a monotonic fashion. That is, if two variables are monotonically related, it will be result 1 or -1 even though their relationship is not linear. Hence, it is capable of capturing non-linear trends between the two signals. The difference between the Pearson and spearman correlation is shown in the Figure 2.

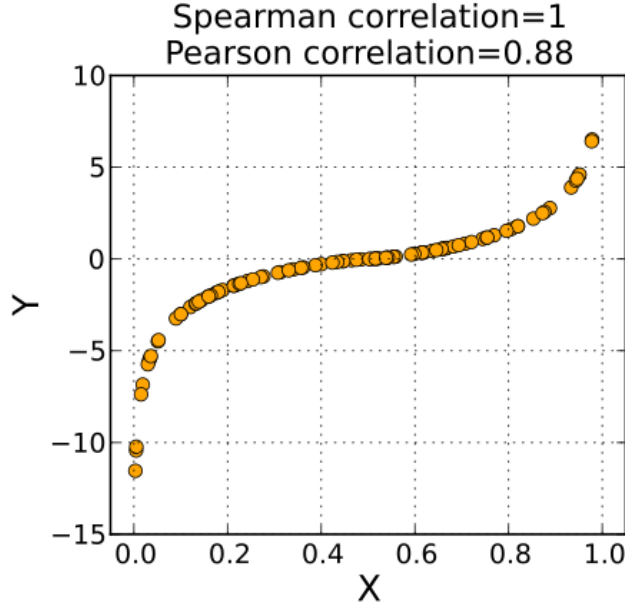


Figure 2: Spearman and pearson correlation between X and Y [65].

Mutual information ( $MI$ ) is another method to calculate the non-directional coupling between two variables.  $MI_{XY}$  between two variables ( $X, Y$ ) can be seen as the amount of extra information needed to transmit  $X$  and  $Y$  from one point to another if we assume  $X$  and  $Y$  are independent of each other [14]. It is denoted as

$$MI_{XY} = \sum_{x \in X, y \in Y} p(x, y) \log \frac{p(x, y)}{p(x)p(y)} \quad , \quad (2)$$

where  $p(x, y)$  is the joint probability distribution between  $X$  and  $Y$ , and  $p(x)$  and  $p(y)$  are the individual probability distributions of  $X$  and  $Y$ , respectively. The product of  $p(x)$  and  $p(y)$  denotes the amount of information transferred assuming both the processes are independent. The  $MI$  is a symmetric function therefore no directional information can be derived from it. The probability distribution can be estimated by using parametric or non-parametric means. If two variables are independent, then the  $MI = 0$  (equation (3)) and on the other hand, if they are highly correlated with each other then it is given by equation (4).

$$\begin{aligned} MI_{XY} &= \sum_{x \in X, y \in Y} p(x, y) \log \frac{p(x)p(y)}{p(x)p(y)} \\ &= 0 \quad , \quad p(x, y) = p(x)p(y) \in X \perp\!\!\!\perp Y \end{aligned} \quad (3)$$

$$MI_{XY} = \sum_{x \in X, y \in Y} p(y) \log \frac{1}{p(x)} \quad , \quad (4)$$

where,

$$p(x, y) = p(x/y) * p(y) \text{ and}$$

$$p(x/y) = 1 \in x \text{ and } y \text{ highly related to each other.}$$

Thomas Schreiber, in his work [16], introduced the time lag in the symmetric function of Mutual Information to add the directional aspect into the equation and came up with the concept of Transfer Entropy (TE). Which is denoted as

$$TE_{x \rightarrow y} = \sum_{x_i \in X, y_i \in Y} p(x_i, x_i^{k-}, y_i^{l-}) \log \frac{p(x_i | y_i^{l-}, x_i^{k-})}{p(x_i | x_i^{k-})} \quad , \quad (5)$$

$$TE_{y \rightarrow x} = \sum_{x_i \in X, y_i \in Y} p(y_i, y_i^{l-}, x_i^{k-}) \log \frac{p(y_i | x_i^{k-}, y_i^{l-})}{p(y_i | y_i^{l-})}. \quad (6)$$

Where  $TE_{x \rightarrow y}$  and  $TE_{y \rightarrow x}$  denote the flow of information from variable  $X$  to variable  $Y$ , and variable  $Y$  to  $X$ , respectively. Moreover,  $x_i, y_i, x_i^{k-}$  and  $y_i^{l-}$ , denotes current value of  $X$ , current of value  $Y$ , past  $k$  values of  $x_i$  and past  $l$  values of  $y_i$ , respectively.

To evaluate the Transfer Entropy (TE) we have to first estimate the probability distribution functions (pdf). We can estimate the pdf using parametric and non-parametric methods as suggested in the paper [27]. The non-parametric method does not make any prior assumptions on the characteristics of the given data whereas the parametric method assume some distribution of the data or fix certain properties of the model. The non-parametric methods such as nearest neighbour and binning [27][45], become computationally expensive when we consider more signals effect or increases the past values that is,  $l$  and  $k$  in the equations (5) and (6). Therefore we have implemented parametric method of transfer entropy to calculate the interactions between the variables. Under the gaussian assumption on the distribution of  $X$  and  $Y$  the original formulation of GC [3] and the transfer entropy is equivalent [32].

GC is capable of detecting linear coupling between the variables. It can be extended to non-linear case by introducing correlation integral or radial basis kernel functions [27]. The GC captures both direct and indirect links. We have implemented conditional GC [45] that detects only direct causality by considering the effect of all the variables available in the system. The difference between indirect and direct causalities is shown in Figure 3, where  $X$  is causing  $Y$ ,  $Y$  is causing  $Z$ , but  $X$  and  $Z$  do not cause each other. In this thesis, we worked on the linear version of conditional GC.

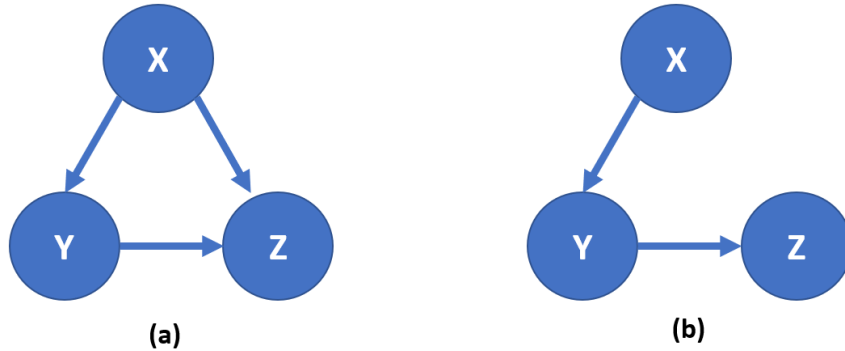


Figure 3: "Indirect causality vs direct causality" when  $X$  is causing  $Y$ ,  $Y$  is causing  $Z$ , but  $X$  and  $Z$  do not cause each other. (a) Indirect causality network obtained without conditional GC method (b) Direct causality network obtained with conditional GC method.

The GC is increasingly used to examine the interactions between the signal in biomedical systems with several applications [51]. Gopikrishna et.al., used multivariate GC in functional magnetic resonance imaging (fMRI) data to investigate the dynamics of brain network [33]. Michal et.al., investigated the interactions between the blood pressure (BP) and RR interval with subjects in resting position, performing mental activities, tilted in the head-up position, and performing mental arithmetics while standing, and concluded that causal interactions varies with different physiological conditions [53]. Faes et.al., studied the linear and non-linear interactions between the heart and brain, and between brain-brain signals during the sleep [46].

### 1.3 Simple Examples

We simulated three different cases of already known relationships to illustrate the difference between causal and non-causality. The first one shows the relationship between the non-causal measure (MI and correlation) and causal measure (GC) for two independent variables. The second one signifies the benefit of using causal measure over non-causal in two linearly coupled variables. In the last one, we have shown that GC fails to detect the

causality between the two non-linearly coupled signals.

### 1.3.1 Two independent Process

Let's consider two independent signals ( $X_1$  and  $X_2$ ) that are denoted as

$$\begin{aligned} X_{1,n} &= W_{1,n} \\ X_{2,n} &= W_{2,n} \quad \in \quad W_1, W_2 \sim \mathcal{N}(0, 1). \end{aligned} \quad (7)$$

Where  $X_{1,n}$  and  $X_{2,n}$  are the current instances of the signal  $X$  and  $Y$ . Each instances are sampled randomly from the Gaussian distribution with mean 0 and standard deviation 1. In this case, the mutual information, correlation, GC all are approximately equal to zero.

### 1.3.2 Two Linearly Coupled Signals

Let's consider two signals ( $X_1$  and  $X_2$ ) that are denoted as

$$\begin{aligned} X_{1,n} &= W_{1,n} \\ X_{2,n} &= 0.4 * X_{2,n-1} + 0.5 * X_{1,n-1} + W_{2,n} \quad \in \quad W_1, W_2 \sim \mathcal{N}(0, 1). \end{aligned} \quad (8)$$

Here  $X_{2,n}$  depends on its and  $X_{1,n}$  past value. Therefore, there is a causal relationship from  $X_1 \rightarrow X_2$  but no causal relationship from  $X_2 \rightarrow X_1$ . In this case, the mutual information and correlation (lag=0) are close to zero. That is, they failed to detect the interaction between these two signals. Whereas, the GC from  $X_1$  to  $X_2$  is significant and nonzero, and from  $X_2$  to  $X_1$  is zero.

### 1.3.3 Two Non-Linearly Coupled Signals

Let's consider two signals ( $X_1$  and  $X_2$ ) that are denoted as

$$\begin{aligned} X_{1,n} &= W_{1,n} \\ X_{2,n} &= 0.4 * X_{2,n-1} + 0.5 * X_{1,n-1}^2 + W_{2,n} \quad \in \quad W_1, W_2 \sim \mathcal{N}(0, 1). \end{aligned} \quad (9)$$

Here  $X_{2,n}$  depends on its and non-linearly on  $X_{1,n}$  past value. Therefore, there is a causal relationship from  $X_1 \rightarrow X_2$  but no causal relationship from  $X_2 \rightarrow X_1$ . In this case, the mutual information and correlation (lag=0) are close to zero. That is, they failed to detect the interaction between these two signals. Also, the GC in both the directions are zero. That is, GC failed to detect the non-linear coupling.

## 1.4 Contribution

The major contribution of this work is to use conditional GC to investigate the causal relationships between the ECG and respiration derived parameters. Even though the GC is actively used in the medical and financial domains, it is the first time that the causal connectivity within and between, ECG and respiration derived parameters systems are investigated to find differences caused by chemicals' exposure. Further, we have used the GC to evaluate the coupling between two unequally sampled signals with the cardinality constraint to accommodate more variables without the explicit need for a large sample size.

## 1.5 Overview

This report is divided into 7 main chapters:

- Chapter 1 discusses the problem at hand, the concept of causality with simple examples, and the contribution of this assignment.
- Chapter 2 describes the formulation of conditional GC in detail for both equal and unequal sampled variables. It explains the methods to decide the model order and ways to carry out coupling significance tests. Latter, we simulate simple examples to show the causal study in practice.
- Chapter 3 presents a description of the data, preprocessing methods and strategy to put everything into practice.

- Chapter 4 showcases the pipeline of developing the prediction model based on causal features.
- Chapter 5 presents the result of this work. It contains the interaction insights and classification results.
- Chapter 6 summarizes the main conclusion of this thesis. The limitations and possible future work are also thoroughly discussed.

Figure 4 briefly shows the steps with the methods involved in the thesis.

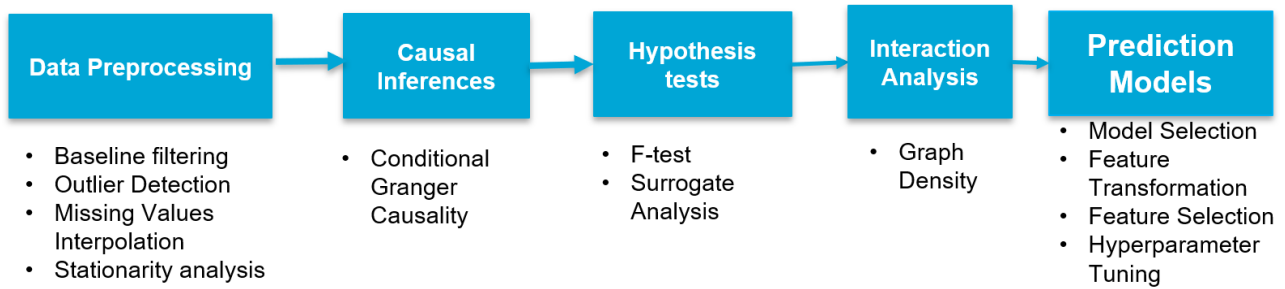


Figure 4: Sequence of steps followed in this assignment.

## 2 Granger Causality: Algorithms and Simulations

In this chapter, the mathematical formulation of Granger Causality and other key concepts are discussed that are necessary to evaluate direct causality. In section 2.1, equal and unequal sampled GC are explained along with the model order selection techniques and least angle regression algorithm. In section 2.2, F-test and surrogate analysis are defined for detecting false causalities statistically. In section 2.3, three simulations are illustrated to showcase the applicability of the concepts to already known cases.

### 2.1 Granger Causality estimation

#### 2.1.1 Mathematical Formulation

GC causal influence based on prediction via multi vector auto-regression (MVAR). According to the definition of GC in [32], the conditional GC for the system consists of three variables ( $X$ ,  $Y$  and  $Z$ ), it is said that “ $Y$  G-causes  $X$ ” if, in an appropriate statistical sense,  $Y$  assists in predicting the future of  $X$  beyond the degree to which  $X$  and  $Z$  already predict  $X$  future. In this thesis we have adopted the notation from the research paper by Montalto et.al [45].

Let’s consider a system described by the set of three variables ( $X$ ,  $Y$  and  $Z$ ). We are interested in evaluating the information flow in the system from source variable  $X$  to the destination variable  $Y$ . The GC assumes the variables to be stationary in nature. That is, the variables should have constant variance over time, should have constant autocorrelation structure over time, have no trend and, no periodic fluctuations. Accordingly we assume  $X, Y$  and  $Z$  as the stationary variables. Moreover, we denote

$$\begin{aligned} X_n^{k-} &= [X_{n-1}, X_{n-2}, \dots, X_{n-k+1}] \\ Y_n^{l-} &= [Y_{n-1}, Y_{n-2}, \dots, Y_{n-l+1}] \\ Z_n^{j-} &= [Z_{n-1}, Z_{n-2}, \dots, Z_{n-j+1}], \end{aligned} \quad (10)$$

where  $X_n^{k-}, Y_n^{l-}, Z_n^{j-}$  are the vector variables representing the past of the variable  $X$ ,  $Y$  and  $Z$  with  $k$ ,  $l$  and  $j$  as the past values ( or time lags), respectively. Furthermore,  $X_n, Y_n, Z_n$  represent the present value of  $X$ ,  $Y$  and  $Z$ , respectively.

Further, we introduce full and reduced vector as  $V^{(u)}$  and  $V^{(r)}$ , respectively for evaluating the information flow from source variable  $X$  to the destination variable  $Y$ .  $V^{(u)}$  contains the past information of  $X$ ,  $Y$  and  $Z$ , and  $V^{(r)}$  contains the past information of  $Y$  and  $Z$  as

$$\begin{aligned} V_n^{(u)} &= [X_n^{k-} \ Y_n^{l-} \ Z_n^{j-}]^T \\ V_n^{(r)} &= [Y_n^{l-} \ Z_n^{j-}]^T. \end{aligned} \quad (11)$$

Then, an unrestricted regression of  $Y_n$  on the full vector and a restricted regression on  $Y_n$  on the reduced vector are performed as

$$\begin{aligned} Y_n &= A^{(u)} V_n^{(u)} + e_{n,YXZ}^u \\ Y_n &= A^{(r)} V_n^{(r)} + e_{n,YZ}^r, \end{aligned} \quad (12)$$

where  $A^{(u)}$  and  $A^{(r)}$  are vectors of linear regression coefficients. The terms  $e_{n,YXZ}^u$  and  $e_{n,YZ}^r$  are scalar white noises with variance  $\sigma_{YXZ}^u$  and  $\sigma_{YZ}^r$ , respectively. The subscript in  $\sigma$  signifies variables whose past information are taken in the equation and additionally the first subscript in  $\sigma$  signifies the target variable. Then the GC value from  $X$  to  $Y$  is given by

$$GC_{XY} = \log \frac{\sigma_{YXZ}^u}{\sigma_{YZ}^r}. \quad (13)$$

Similarly, the information flow in the system from source variable  $Y$  to the destination variable  $Z$  is given by

$$GC_{YZ} = \log \frac{\sigma_{ZYX}^u}{\sigma_{ZX}^r}. \quad (14)$$

The notation of all the possible interactions is shown in Figure 5.

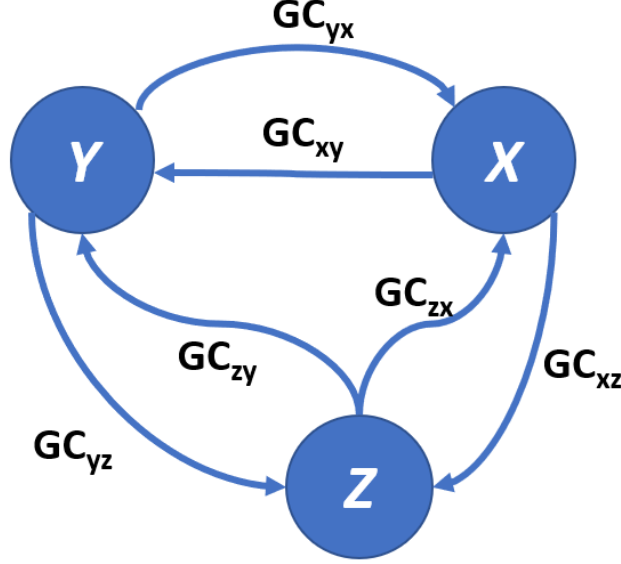


Figure 5: Interactions notations between the three variables system.

In the next section we extend the above formulation of GC to estimate causality between two unequal sampled signals.

### 2.1.2 Calculation Granger Causality in unequal sampled signals

The variables derived from ECG and respiration signal are unequally spaced with respect to the time. For the evaluation of interactions between the ECG and respiration system, the old GC mathematical formulation will not work. That is, previously discussed mathematical formulation is only correct when all the variables of the system are evenly sampled. But still, we can have the same notion of GC. That is, how well a past occurrences certain variable (say  $X$ ) assists in predicting future instances of another variable (say  $Y$ ) beyond the degree to which the past occurrences of  $Y$  already predicts  $Y$  future.

Let's consider two sampling function  $h_X$  and  $h_Y$  of two different variable  $X(a)$  and  $Y(t)$ , respectively. Where  $X$  is sampled at lower rate than  $Y$ , see Figure 6 for an example.

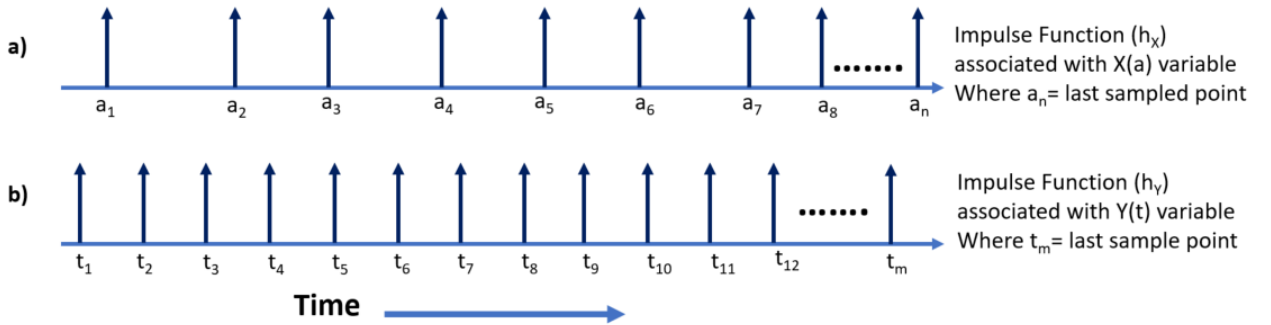


Figure 6: Sampling impulse response of variable  $X$  and  $Y$

Moreover,  $X(a)$  and  $Y(t)$  at any instant  $a_i$  and  $t_i$  can be sampled by using a sampling function denoted as

$$\begin{aligned} X(a_i) = X(a) * h_X(a - a_i), \quad \in h_X(a - a_i) = 1, \quad a_i \in a_1, a_2, \dots, a_n \\ = 0, \quad a_i \notin a_1, a_2, \dots, a_n \end{aligned} \quad (15)$$

$$\begin{aligned} Y(t_i) = Y(t) * h_Y(t - t_i), \quad \in h_Y(t - t_i) = 1, \quad t_i \in t_1, t_2, \dots, t_m \\ = 0, \quad t_i \notin t_1, t_2, \dots, t_m. \end{aligned} \quad (16)$$

We are interested in evaluating the information flow in the system from source variable  $X$  to the destination variable  $Y$ . We denote

$$\begin{aligned} X_{a_j}^{p-} &= [X_{a_{j-1}}, X_{a_{j-2}}, \dots, X_{a_{j-p+1}}] \\ Y_{t_i}^{p-} &= [Y_{t_{i-1}}, Y_{t_{i-2}}, \dots, Y_{t_{i-p+1}}] \\ a_{j-p+1} &< a_{j-p} < \dots < a_{j-2} < a_{j-1} < t_i, \end{aligned} \quad (17)$$

with  $X_{a_j}^{p-}, Y_{t_i}^{p-}$  as the vector variables representing the past  $p$  past values of the variable  $X$  and  $Y$ , respectively. Furthermore,  $Y_{t_i}$  represents current value of  $Y$ .

Further we introduce, full and reduced vector as  $V^{(u)}$  and  $V^{(r)}$ , respectively for evaluating the information flow from source variable  $X$  to the destination variable  $Y$ .  $V^{(u)}$  contains the past information of  $X$  and  $Y$ , and  $V^{(r)}$  contains the past information of  $Y$  only as

$$\begin{aligned} V_n^{(u)} &= [X_{a_j}^{p-} \ Y_{t_i}^{p-}]^T \\ V_n^{(r)} &= [Y_{t_i}^{p-}]^T. \end{aligned} \quad (18)$$

Then, an unrestricted regression of  $Y_{t_i}$  on the full vector and a restricted regression on  $Y_{t_i}$  on the reduced vector are performed as follows:

$$\begin{aligned} Y_{t_i} &= A^{(u)} V_n^{(u)} + e_{n,YX}^u \\ Y_{t_i} &= A^{(r)} V_n^{(r)} + e_{n,Y}^r, \end{aligned} \quad (19)$$

where  $A^{(u)}$  and  $A^{(r)}$  are vectors of linear regression coefficients. The terms  $e_{i,YX}^u$  and  $e_{i,Y}^r$  are scalar white noises with variance  $\sigma_{YX}^u$  and  $\sigma_Y^r$ , respectively. The subscript in  $\sigma$  signifies variables whose past information are taken in the equation and additionally the first subscript in  $\sigma$  signifies the target variable. Then the GC value from  $X$  to  $Y$  is given by

$$GC_{XY} = \log \frac{\sigma_{YX}^u}{\sigma_Y^r} \quad (20)$$

Similarly we define below set of equations to evaluate the information flow in the system from source variable  $Y$  to the destination variable  $X$ .

$$\begin{aligned} X_{a_j}^{p-} &= [X_{a_{j-1}}, X_{a_{j-2}}, \dots, X_{a_{j-p+1}}] \\ Y_{t_i}^{p-} &= [Y_{t_{i-1}}, Y_{t_{i-2}}, \dots, Y_{t_{i-p+1}}] \\ t_{i-p+1} &< t_{i-p} < \dots < t_{i-2} < t_{i-1} < a_j. \end{aligned} \quad (21)$$

As compared to the previous case, this time  $p$  recent past samples of  $Y$  are considered whose occurrence time is lesser than current  $X$  instance. Similarly, we defined full and reduced as  $V^{(u)}$  and  $V^{(r)}$ , respectively. Where,  $V^{(u)}$  contains the past information of  $Y$  and  $X$ , and  $V^{(r)}$  contains the past information of  $X$  only as

$$\begin{aligned} V_n^{(u)} &= [X_{a_j}^{p-} Y_{t_i}^{p-}]^T \\ V_n^{(r)} &= [X_{a_j}^{p-}]^T, \end{aligned} \quad (22)$$

Then, an unrestricted regression of  $X_{a_j}$  on the full vector and a restricted regression on  $X_{a_j}$  on the reduced vector are performed as follows:

$$\begin{aligned} X_{a_j} &= A^{(u)} V_n^{(u)} + e_{n,XY}^u \quad \text{unrestricted regression} \\ X_{a_j} &= A^{(r)} V_n^{(r)} + e_{n,X}^r \quad \text{restricted regression .} \end{aligned} \quad (23)$$

Granger Causality value from  $Y$  to  $X$  is given by

$$GC_{YX} = \log \frac{\sigma_{YX}^u}{\sigma_X^r} \quad (24)$$

Before evaluating GC, we need to estimate the past lag values or model order for both restricted and unrestricted equations. Model order estimation techniques are discussed in the next section. The statistical significance of the GC estimated through the autoregression technique is discussed in section 2.2.

### 2.1.3 Model Order Selection

The estimation of GC requires the number of time-lags or past values of the variable. In our three variables system,  $k, l, j$  represent this. We have used uniform embedding. That is, the number of past values of all variables is considered the same. We defined model order ( $p$ ) as equal to the past values considered for each of the variables in GC equations. Small model order could lead to the problem of curse of dimensionality [1] and large model order could lead to the problem of underfitting [58]. One way is to increase the model order until the fitting error is minimized. The major problem with this approach is that the error is a monotonically non-increasing function of the model order  $p$ . This issue can be overcome by integrating a penalty function that increases with the model order. Two popular criteria: the Akaike information criterion ( $AIC$ ) [6] and the Bayesian information criterion ( $BIC$ ) [4], are suggested that effectively penalizes the objective function as the model order increases. The formulation of AIC and BIC are denoted as

$$\begin{aligned} AIC(p) &= 2p - 2 \log(L) \\ BIC(p) &= \log(n)p - 2 \log(L) \quad , \end{aligned} \quad (25)$$

where  $p, L$  and  $n$  are model order, error(loss) and the number of training samples, respectively. Given the set of models with different model orders, the preferred model is the one with the minimum AIC and BIC values. For short data sequences, none of the above criteria tends to work particularly well [5]. Therefore, these criteria are only be used as "indicators" or initial guesses of the model order. The Figure 7 shows AIC and BIC plots that are evaluated of a ECG link in healthy phase for two random subjects. According to the figure, the past lag value equal to 5 satisfies both the cases.

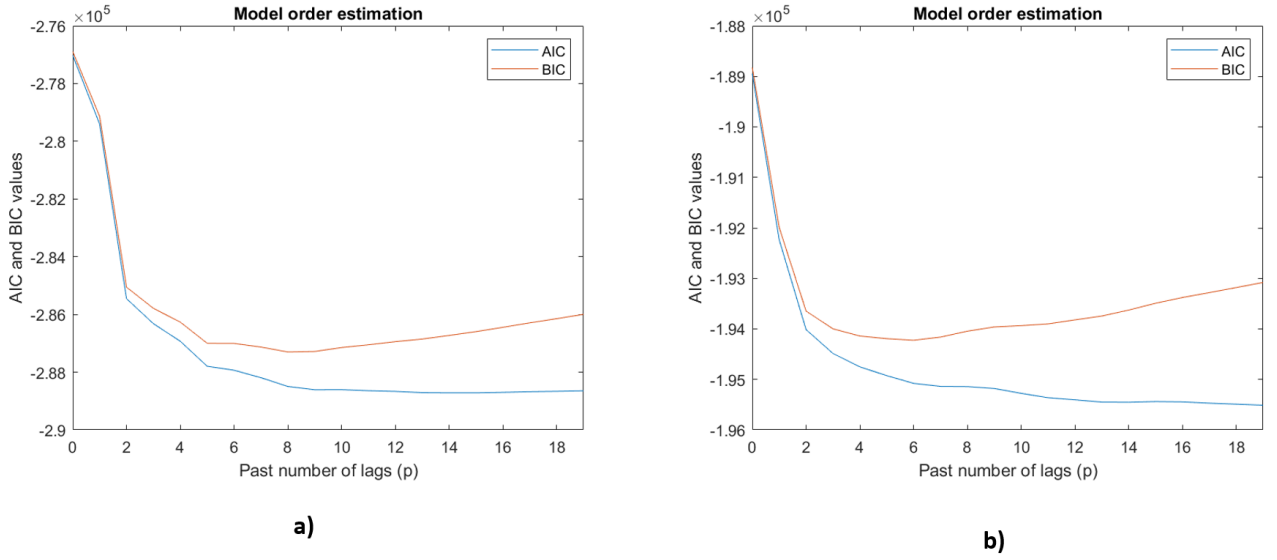


Figure 7: AIC and BIC are calculated with respect to the model orders for a ECG link in healthy phase for two random subjects. The model order equal to 5 seems to satisfy both the subjects.

#### 2.1.4 Solving Regression Equation

To evaluate Granger causalities, we have to estimate  $A^{(u)}$  and  $A^{(r)}$  coefficients of unrestricted and restricted regression equations, respectively (refer the equation (23)). That is, we need to solve two regression equations for each of the interactions.

Let us consider a regression equation as

$$Y_n = A * V_n + e_n, \quad (26)$$

where  $Y_n$  is the present value of  $Y$ ,  $A$  is a row vector of representing regression coefficients,  $V_n$  is a column vector containing past  $p$  instances of  $m$  different variables each and  $e_n$  is a white noise with variance  $\sigma$ .  $V_n$  for three variables case ( $X, Y, Z$ ) is denoted as

$$V_n = [X_n^{p-} \ Y_n^{p-} \ Z_n^{p-}]^T. \quad (27)$$

We could estimate  $A$  vector by solving the objective function (28) using least-square estimation technique [34].

$$\text{minimize } L(A) = (1/2N) \sum_{n=1}^{n=N} \|Y_n - A * V_n\|_2^2, \quad A \in R^{mp \times 1}. \quad (28)$$

The dimension of the regression equation (26) or the length of vector  $A$  increases as we incorporate more variables into the equation (26) for fixed  $p$ . Without enough samples, the modelling will suffer the problem of curse of dimensionality [1].

To solve the regression equation (26) with relatively smaller sample size, we introduced the L-1 norm or sparsity regularization in the objective function (28) as follows,

$$\text{minimize } L(A) = (1/2N) \sum_{n=1}^{n=N} \|Y_n - A * V_n\|_2^2 + \alpha \|A\|_1, \quad A \in R^{mp \times 1}, \quad (29)$$

where  $\alpha$  is the regularization term that signifies the importance of L-1 norm. The larger the value of  $\alpha$ , the simpler the model will be.

To solve the objective function (29) Least Angle regression(LARS) is used. Least Angle Regression is an algorithm that effectively solves high dimensional regression models (i.e model with lot of features) [20]. LARS is similar to forward stepwise regression. At each iteration LARS choose the feature which is most correlated to the target variable. There may be a case when more than one features are equally correlated. In such scenario, LARS averages the same correlated features and advances in a direction in between the directions corresponding to each of the same correlated features. LARS bounces in the space in the most optimally calculated direction without overfitting the model.

LARS works as follows as [19]

- All coefficients of feature vector is set to zero.
- The feature is selected that is most correlated to residual.(Residual is the difference between the observed value and the predicted value)
- The coefficient corresponding to selected feature is updated from 0 in the direction that is most correlated with residual
- Previous step is stopped as soon as another feature has equal or higher correlation with residual than the selected feature.
- In case of equal correlation, update both the features in the direction defined by their joint least square coefficient of the current residual, until some other feature has as much correlation with the current residual.
- Continue until reduction of residual is no more significant or until all the features are in the model.

The level sets of norm-1 and norm-2 are shown in Figure 8 for two-variable case.

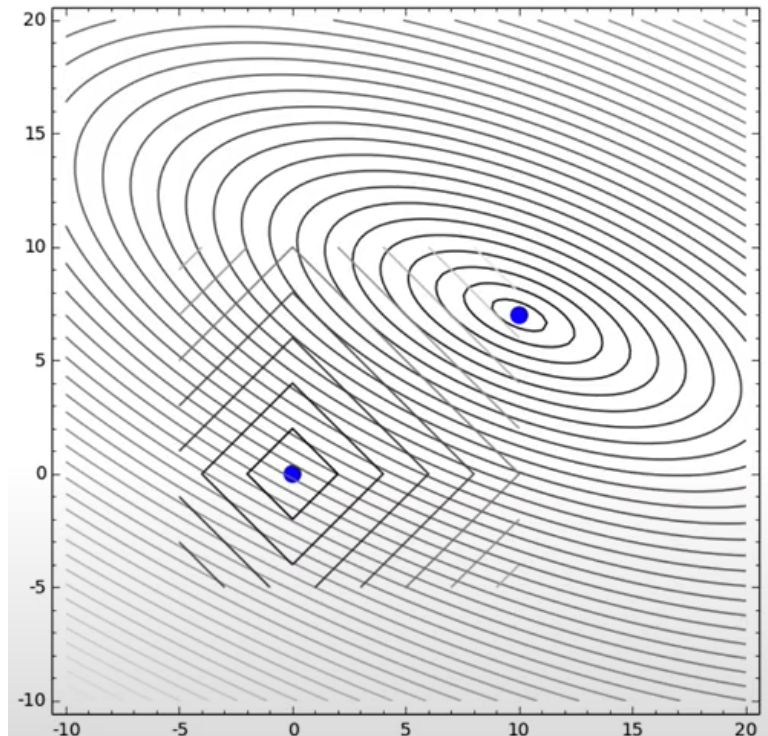


Figure 8: Level sets of norm-1 and norm-2 for two-variable case

In Figure 8, the blue point in the lower left is the zero model or the simplest model. The blue point upper right is the model that minimizes the L-2 norm or most accurate model. As  $\alpha$  increases, the estimated model from the objective function (29) will move closer to the lower left blue point. We want to find the best alpha such

that the intersection between the two-level set is closer to the upper blue point. To achieve this, we use 5-fold cross-validation to estimate the best alpha.

In Figure 8, the LARS algorithm will start at the lower left point and will move vertically up till the third norm-1 level set. Because at the third level set, there is a tangential intersection between the norm-1 and norm-2 level set. That is another variable now become also highly correlated with the residual. Hence, now the weights will get updated in the direction of 45 degrees to the upper blue point.

## 2.2 Statistical analysis

The statistical significance of the coupling values is assessed by F-tests and surrogate analysis, both the approaches are discussed in subsequent chapters. Checking the significance is necessary to discard false causalities.

### 2.2.1 F test

The statistical significance of the GC estimated by regression equations is checked by a parametric F-test for the null hypothesis [3]. Here null hypothesis represents no significant direct causal link between the two variables. We evaluate whether the GC value between the two variables is significant or a random guess.

Let's consider set of the GC equations as

$$\begin{aligned} \text{H1: Unrestricted Model } Y_n &= A^{(u)}V_n^{(u)} + e_{n,YXZ}^u, \\ \text{H0: Restricted Model } Y_n &= A^{(r)}V_n^{(r)} + e_{n,YZ}^r. \end{aligned} \quad (30)$$

Where H0 is the null hypothesis which is significant when there is no causal effect from  $X$  to  $Y$ . Otherwise, H1 equation will be significant. The null hypothesis is significant when the estimated errors of H1 ( $e_{n,YXZ}^u$ ) and H0 ( $e_{n,YZ}^r$ ) are comparable. Here we need to test against the null hypothesis. We use F-test to properly assess the significance of the errors difference between the restricted and unrestricted of the equations.

We define the residual sum of square error (RSS) as

$$\begin{aligned} RSS_{UR} &= \sum_{n=1}^N (e_n^u)^2 \\ &= \sum_{n=1}^N (Y_n - \hat{Y}_n^u)^2, \text{ and} \end{aligned} \quad (31)$$

$$\begin{aligned} RSS_R &= \sum_{n=1}^N (e_n^r)^2 \\ &= \sum_{n=1}^N (Y_n - \hat{Y}_n^r)^2, \end{aligned} \quad (32)$$

where  $RSS_{UR}$  and  $RSS_R$  are the residual sum of square errors for unrestricted and restricted models, respectively. The  $\hat{Y}_n^u$  and  $\hat{Y}_n^r$  are the predicted value of  $Y_n$  for unrestricted and restricted models, respectively. Finally,  $N$  is the total number of samples.

In this case F test statistics is defined as

$$F \text{ value} = \frac{RSS_R - RSS_{UR}}{\frac{RSS_{UR}}{N - mp}}, \quad (33)$$

where  $m$  is the total number of variables in the system and  $p$  is the number of past values considered for each of the variables  $F$  value is the ratio of two chi square distribution with degree of freedom  $p$  and  $N - mp$ , respectively. Here we assume that the residual error has Gaussian distribution. The GC is considered statistically significant

if the  $F$  value is greater than the  $F$  critical, calculated from the Fisher distribution with  $(p, N - mp)$  degrees of freedom at the significance level  $\alpha = 0.05$ .

Another way to understand the link between the  $F$  value and GC is by analyzing the size of denominator and numerator of equation (33). For the link to be significant, the numerator and denominator of equation (33) should be large and small, respectively. That is, the difference between the  $RSS_R$  and  $RSS_U$  should be large, and at the same time,  $RSS_U$  should be small. In such a case, the restricted model performs worse than the unrestricted model. Therefore adding a variable into the system will improve the prediction accuracy, (unrestricted model) that implies a significant information flow from past values of the added variable to the target variable.

### 2.2.2 Surrogate Analysis

Surrogate analysis technique can also be used to check the statistical significance of the GC [17]. Surrogate analysis statistically evaluates the importance of using non-linear approaches to model the data. It is also used for checking the significance of synchronization or linear and non-linear coupling between two signals.

In surrogate analysis, we generate the data from the original data that have the same and different properties. Different properties are the properties that we want to test against. It is highlighted in the null hypothesis. The null hypothesis is what we want to reject using discriminating statistics. The null hypothesis is tested using generated surrogate data. Some examples of the null hypothesis

- No coupling between the signals
- Signal is explained well by linear model
- There is no synchronization between the signals

If the value of the discriminating statistic of the surrogate data is significantly different from the original data, then we reject the null hypothesis. Some examples of discriminating statistic

- Average residual error: Used for checking between linear and non-linear model
- GC value : Used for checking Coupling
- Correlation values: Used for checking random signal

Let's consider a signal  $X$  modeled as

$$X_n = -0.5562 * X_{n-1} - 0.9^2 * X_{n-2} + w_X, \quad (34)$$

$$w_X \sim \mathcal{N}(0, 1).$$

Where current value of  $X$  depends on its previous two values. Here our aim is to prove that variable is not random. The auto- correlation of random variable is close to zero for lag greater than 0. The auto-correlation sequence of random signal does not change after its random shuffling. Hence we can use lag-1 correlation value for discriminating analysis.

In the Figure 9, the distribution of the surrogate of  $X$  does not change but the lag-1 correlation has changed. Therefore we concluded that the signal  $X$  is not random and, we reject the null hypothesis.

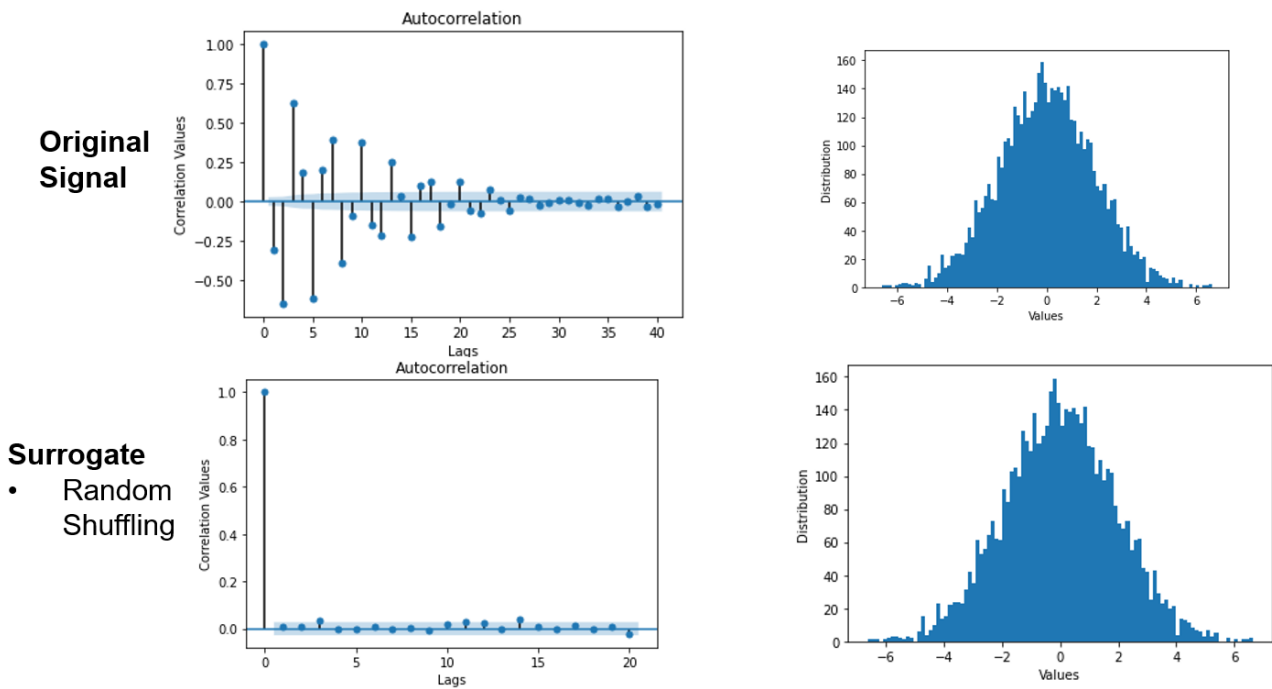


Figure 9: The correlation and distribution of the surrogate of X generated by random shuffling. The top row shows the autocorrelation and distribution of the original signal (X), generated by equation (34). The bottom row shows the autocorrelation and distribution of the randomly shuffled X. The distributions of the original signal X and surrogate are the same. There is a significant change in the lag-1 correlation between the original signal and its surrogate; therefore, X is not a random signal.

A brief overview of the null hypothesis, discriminating statistics, and type of surrogate is depicted in Figure 10 that are useful in current and future work.

Test	Non- Linearity	Coupling
<b>Goal</b>	Confirm nonlinearity	Confirm Coupling
<b>Null Hypothesis</b>	Process is Linear	No coupling
<b>Destroy by making Surrogates</b>	Non Linear Dynamics	Coupling relations
<b>Discriminating Statistics</b>	Residual error	Granger Causal (GC)
<b>If null hypothesis is not rejected</b>	Process is Linear	There is no coupling btw signals
<b>If null hypothesis is rejected</b>	Process is not linear (with some probability)	Signals cannot be considered having no coupling (with some probability)

Figure 10: Comparison of key elements of surrogate analysis between Non-Linearity and Coupling

**Different Types of Surrogates** There are basically five types of surrogates that are used to test for linear and non-linear couplings

- **Random Shuffling:** It is primarily the shuffled replica of the signal. It destroys the auto-correlation sequence and keeps the amplitude distribution the same. It is used for testing the randomness of the signal and the coupling between the two signals. For testing coupling, the surrogate of the driver or the target series is taken.
- **Time delay surrogates or shift testing or circular shifting:** The signal is time-shifted with wrapping. The surrogate signal has a different phase that is decreased or increased by the same amount. The correlation, periodogram and amplitude distribution of the signal remain the same [29][45]. The time delay surrogates method test the significance of phase synchronization and coupling between the two signals.
- **Random phase or Fourier Surrogate:** It randomizes the Fourier phase of the signal but keeps the magnitude of its Fourier transforms the same. It results in a different phase and different amplitude distribution but preserves the correlation and periodogram. Fourier Surrogate is applied to the driver or target signal to test the significance of phase synchronization and coupling between the two signals [28].
- **Amplitude Adjusted Fourier Transform (AAFT):** Random Phase surrogates usually have a gaussian distribution. That is, often not true for real data. It may lead to false rejections based on just amplitude distribution. Therefore we need to have same amplitude distribution to avoid false rejections [17][28]. The phase correlations in the signal indicate non-linearity. The AFFT surrogates ensure approximately the same amplitude distribution as the original signal with phase. The magnitude of the Fourier transform, periodogram and correlation of the original signal remains the same with the surrogate. AFFT method tests the significance of non-linearity in the signal and the coupling significance between the two signals [54]. In one of the previous research, causal relationships between the brain waves powers of rats was tested using conditional mutual information and AAFT. Then it was used to differentiate between the shallow and deep anesthesia [37]. In this work, we have used AAFT for the surrogate analysis.
- **Iterative Amplitude Adjusted Fourier Transform (IAAFT):** IAAFT better preserves the power spectrum and amplitude distribution as compared to AAFT. IAAFT is used to tests for non-linearity and coupling [54]. Maiwald et al.,2008 [31] provide a detailed explanation of the algorithm to generate AAFT and IAAFT surrogates. They also compared the performance of AAFT and IAAFT and found out that AAFT performs well than IAAFT.

**Test Design:** One-sided rank order test is used to test the significance of the coupling between the two signals as described by Schreiber et al., [17] and by James Theiler [10]. First, we choose an acceptable probability of occurring false-positive ( $\alpha$ ). According to the general concern  $\alpha = 0.05$  is generally acceptable. Then we evaluate the number of surrogates ( $M$ ) required for the test that is given by

$$M = \frac{K}{\alpha} - 1, \quad (35)$$

Where  $K$  controls the sensitivity of the test. That is, more surrogates will increase the discrimination power between the true signal and the surrogate signal. For the higher value of  $K$ , we need to generate more surrogates resulting in more computational requirements. In this work we used  $K=5$  or  $M = 99$  with  $\alpha = 0.05$ . For the coupling to be significant, the evaluated GC of the true signal should be higher than the evaluated GCs of at least 95 surrogates. Otherwise, we cannot reject the null hypothesis and, we conclude that no significant coupling is there between the signals.

**Simulation:** Let's consider two signal  $X$  and  $Y$  that are generated as

$$\begin{aligned} X_n &= 0.95 * \sqrt{2}X_{n-1} - 0.9025 * X_{n-2} + w_X, \\ Y_n &= 0.6 * X_{n-2} + 0.25 * \sqrt{2} * Y_{n-1} + w_Y, \\ w_X, w_Y &\sim \mathcal{N}(0, 1). \end{aligned} \quad (36)$$

Above equation is depicted in Figure 11 in directed graph form with edge label representing the affecting variable strength.



Figure 11: The depiction of equation (36) in directed graph.

We used the random shuffling, Amplitude Adjusted Fourier Transform (AAFT) and Random phase surrogates to test the significance of the evaluated Granger causality (GC). In each case we compared the original signal GC with the 99 generated surrogates for both side of the link (that is  $Y \rightarrow X$  and  $X \rightarrow Y$ ). The results are shown in figure-12. Where first row and second row represents coupling from  $X \rightarrow Y$  and  $Y \rightarrow X$ , respectively. The orange dot represent the GC of the original signal. In the case of the first row ( $Y \rightarrow X$ ), coupling is not significant because the GC of the original signal is lesser than the most GCs of the surrogates. Whereas, in the second row ( $X \rightarrow Y$ ), the evaluated GC of the true signal is higher than the evaluated GCs of atleast 95 surrogates. Therefore for the second row we can reject the null hypothesis and conclude that, there is a significant link from  $X \rightarrow Y$ .

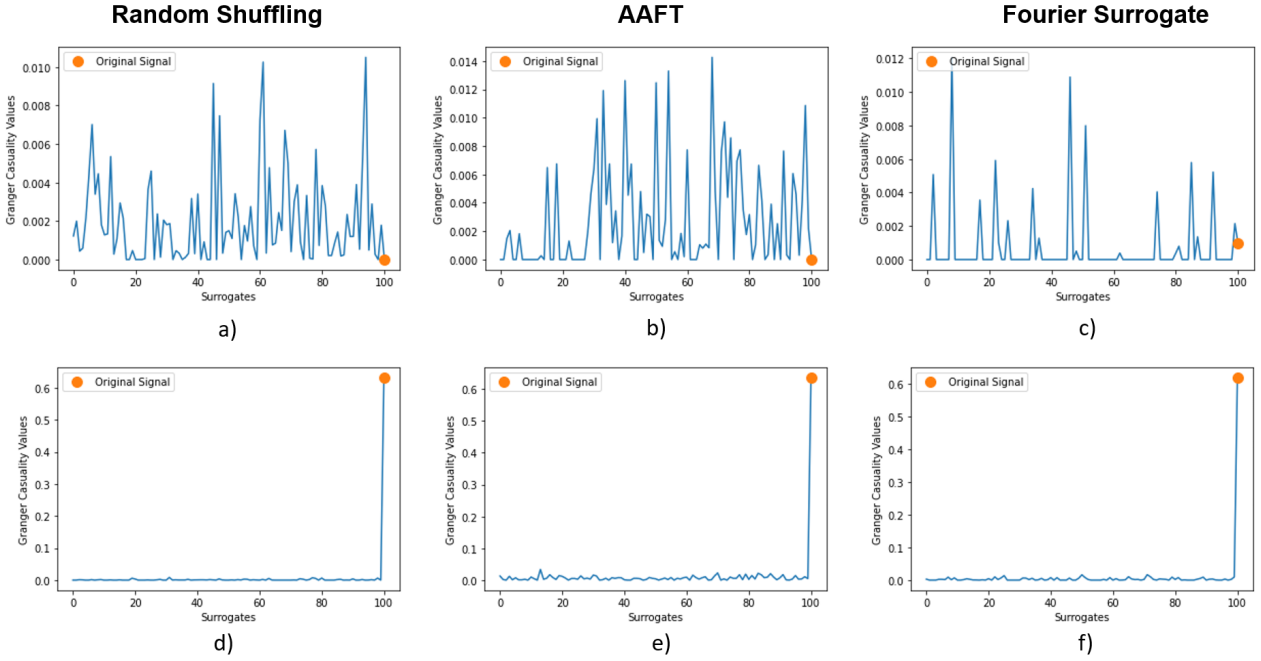


Figure 12: The granger causalities for 99 surrogates are evaluated that are generated by using three different methods. Top row (a,b,c) represent the link  $Y \rightarrow X$  and bottom row (d,e,f) represent the link  $X \rightarrow Y$ . The link  $X \rightarrow Y$  is significant according to all three methods because the red dot( true signal granger causality) is higher than all its surrogates counterparts. While in the case of the link  $Y \rightarrow X$  this is not the case.

## 2.3 Simulation Results

We simulated three different cases of already known coupling to illustrate the applicability of the above concepts. The first one shows the relationship between GC value and coupling strength. The second one signifies the benefit of using cardinality constraint in the objective function over the one without it. In the last one, we have shown that there is no need to resample the unequal sample signals while evaluating GC.

### 2.3.1 Three Variable Case

Let's consider three process X, Y and Z that are created as

$$\begin{aligned}
 X_n &= -0.5562 * X_{n-1} - 0.9^2 * X_{n-2} + w_X \\
 Y_n &= 1.2944 * Y_{n-1} - 0.8^2 * Y_{n-2} + C_{32} * Z_{n-1} + C * X_{n-1} + w_Y \\
 Z_n &= 1.599 * Z_{n-1} - 0.8^2 * Z_{n-2} + C_{23} * Y_{n-2} + (1 - C) * X_{n-2} + w_Z.
 \end{aligned} \tag{37}$$

$$w_X, w_Y, w_Z \sim \mathcal{N}(0, 1)$$

Above equation is depicted in Figure 13 in directed graph form with edge label representing the affecting variable strength.

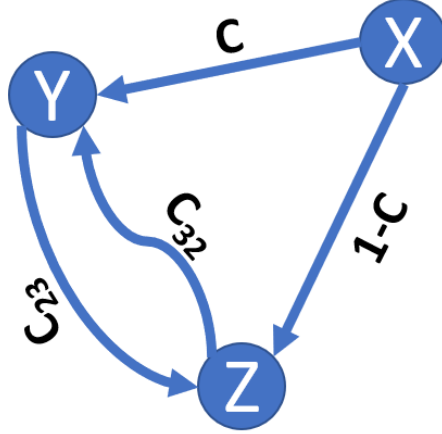


Figure 13: The depiction of equation-37 in directed graph.

The equation (37) is simulated with different values of  $C$ , varied from 0 to 1 in steps of 0.01, keeping the  $C_{23} = 0.1$  and  $C_{32} = 0.5$  constant. As at each  $C$  value the Granger causality between  $X$  to  $Y$  ( $GC_{XY}$ ) and  $X$  to  $Z$  ( $GC_{XZ}$ ) is calculated and plotted in figure-14.

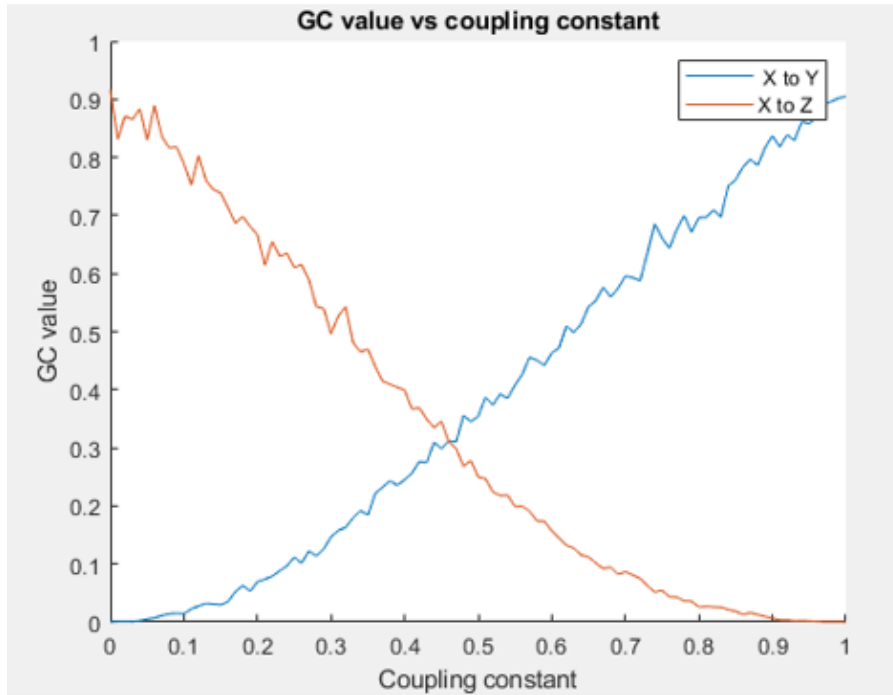


Figure 14: The coupling constant  $C$  is varied from 0 to 1 in steps of 0.01. With the increase in  $C$ , the GC value of the  $X \rightarrow Y$  increases while the GC value  $X \rightarrow Z$  decreases in accordance to the equation-(37).

According to the figure-14, as coupling constant  $C$  increases, the  $GC_{XY}$  also increases and  $GC_{XZ}$  decreases because  $X$  to  $Z$  is affected by  $(1-C)$  coupling constant. The simulation shows that the Granger Causality value is higher for strongly related signals.

### 2.3.2 Eleven Variable Case

Let's consider eleven processes from  $X_1$  to  $X_{11}$  that are created as (following set of equations are taken from the work by Montalto et.al., [45] )

$$\begin{aligned}
X_{1,n} &= 0.95\sqrt{2}X_{1,n-1} - 0.9025X_{1,n-2} + w_{1,n} \\
X_{2,n} &= 0.5X_{1,n-2} + 0.5\sqrt{2}X_{4,n-1} + w_{2,n} \\
X_{3,n} &= -0.3X_{1,n-3} + 0.4X_{3,n-2}w_{3,n} \\
X_{4,n} &= 0.5X_{1,n-2} + 0.25\sqrt{2}X_{4,n-1} + 0.25\sqrt{2}X_{5,n-1} + w_{4,n} \\
X_{5,n} &= -0.25\sqrt{2}X_{4,n-1} + 0.25\sqrt{2}X_{5,n-1} + w_{5,n} \\
X_{6,n} &= 0.5x_{2,n-2} + 0.25\sqrt{2}X_{5,n-1} + w_{6,n} \\
X_{7,n} &= 0.5X_{7,n-1} + X_{1,n-3} + w_{7,n} \\
X_{8,n} &= 0.5X_{8,n-1} + 0.65x_{3,n-3} + w_{8,n} \\
X_{9,n} &= 0.5X_{9,n-1} + 0.4X_{3,n-3} + w_{9,n} \\
X_{10,n} &= 0.5X_{10,n-1} + 0.4X_{9,n-3} + 0.5X_{7,n-1} + w_{10,n} \\
X_{11,n} &= w_{11,n} \quad .
\end{aligned} \tag{38}$$

$$w_{i,n} \sim \mathcal{N}(0, 1) \quad , i \in 1, 2, 3, \dots, 11$$

Where  $w_{i,n}$  is random independent IID process which is Gaussian distributed. Note that  $X_{11}$  is a IID process independent of other variable.

Above equations is depicted in Figure 15 in directed graph.

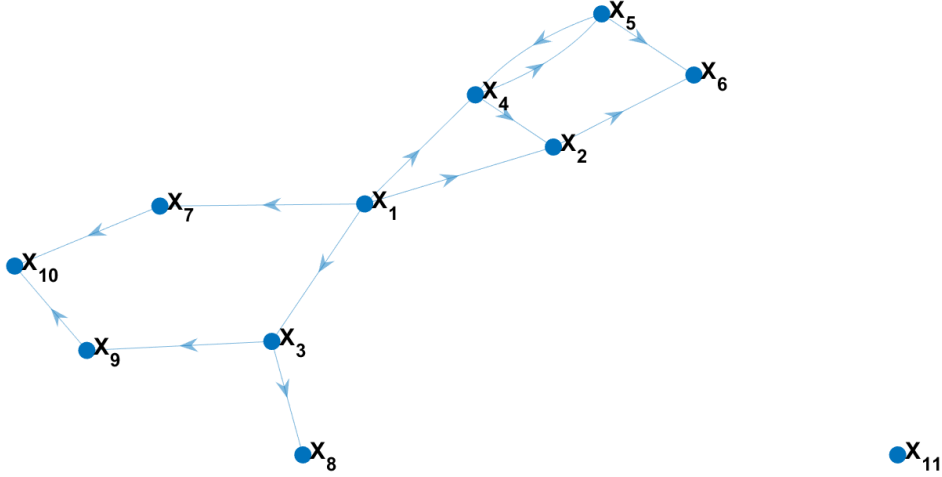


Figure 15: The depiction of equation-38 in directed graph.

The GC between the variables of equation (38) are calculated without and with sparsity constraint for the different number of samples and are shown in Figure 16 and Figure 17, respectively.

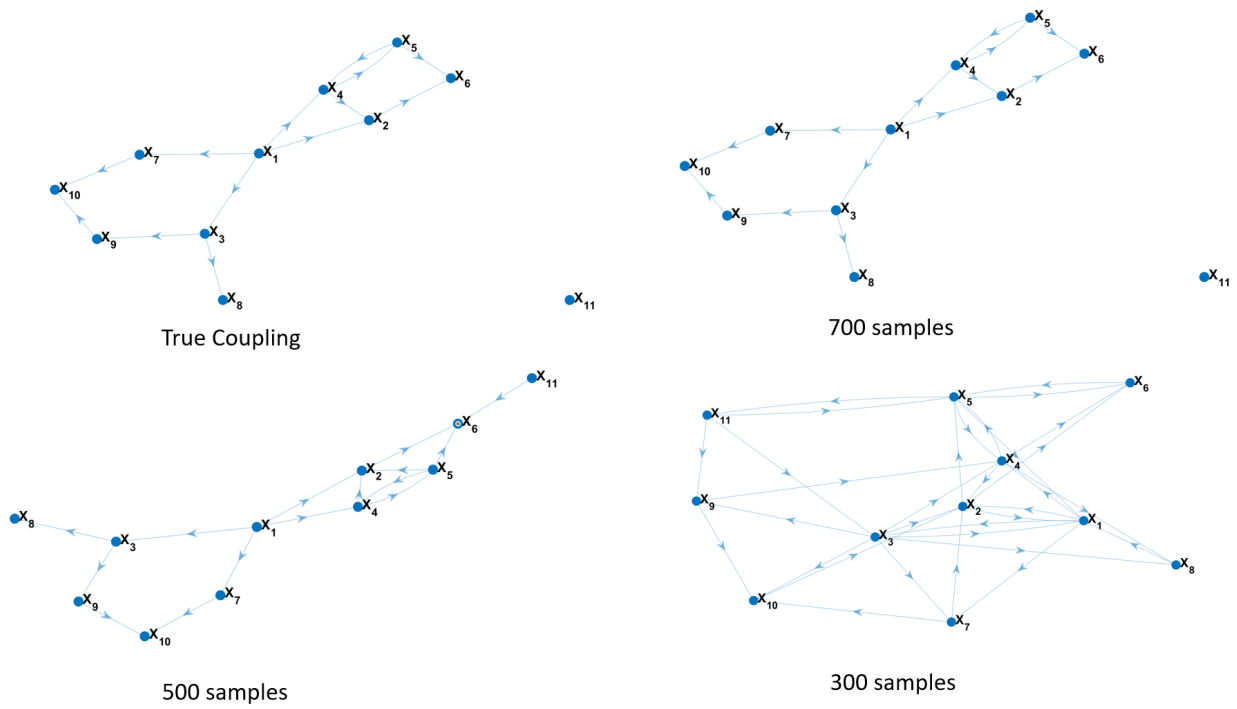


Figure 16: Significant links are evaluated for the different number of samples without sparsity constraint. The upper left graph shows the true coupling. With the decrease in the number of samples, the number of false causalities increases.

The Figure 16 have a lot of false causalities as the number of samples decreases from 700 to 300 samples. This shows that the loss function without sparsity constraint suffers from the curse of dimensionality problem.

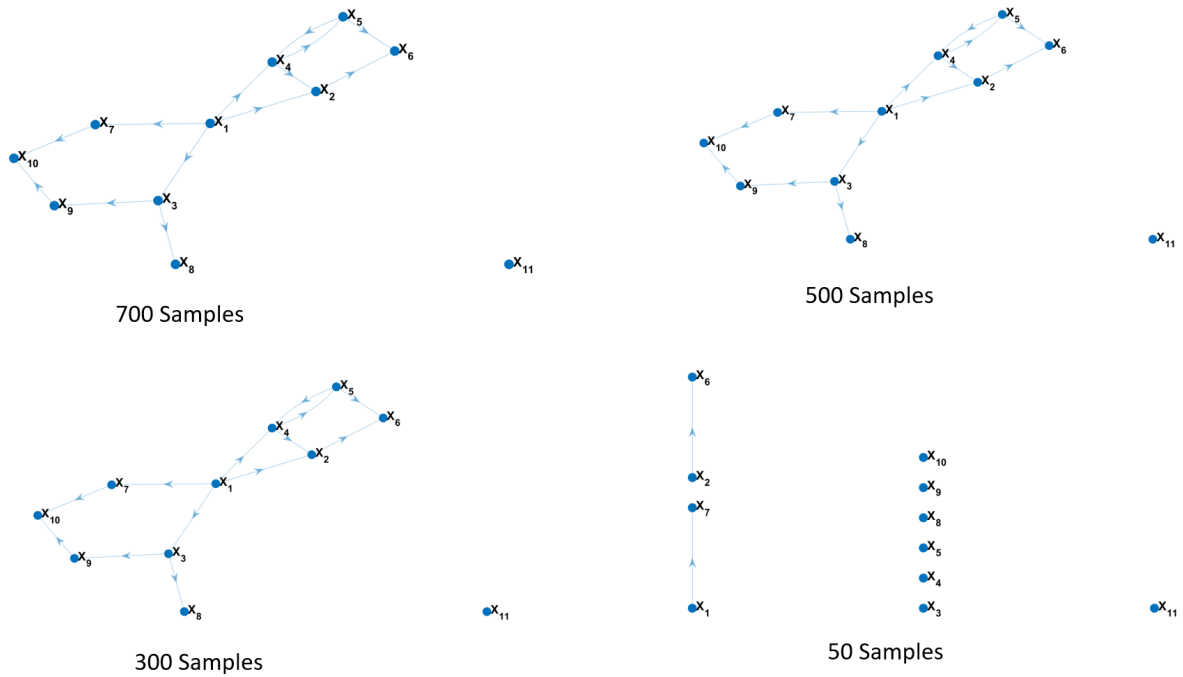


Figure 17: Significant links are evaluated for the different number of samples with a sparsity constraint. No false causalities are detected when we reduced the sample size from 700 to 300 samples. The algorithm with the sparsity constraint for parameter estimation is beneficial over the one without the sparsity constraint.

The Figure 17 as compared to the Figure 16 shows no false causalities when the number of samples is reduced from 700 to 300 samples. This clearly shows that adding the sparsity constraint can effectively evaluate the high dimensional model with relatively smaller sample size.

### 2.3.3 Equal and Unequal Sampled Granger Causality

In this section, we compared the Granger causalities values evaluated through two different methods ( even and uneven) of the unevenly sampled signal.

Lets consider two signal  $X$  and  $Y$  that are sampled at any instant  $a_i$  and  $t_i$ , respectively as

$$\begin{aligned} X_{a_i} = X(a) * h_X(a - a_i), \quad \in h_X(a - a_i) = 1, \quad a_i \in a_1, a_2, \dots, a_n \\ = 0, \quad a_i \notin a_1, a_2, \dots, a_n \end{aligned} \quad (39)$$

$$\begin{aligned} Y_{t_i} = Y(t) * h_Y(t - t_i), \quad \in h_Y(t - t_i) = 1, \quad t_i \in t_1, t_2, \dots, t_m \\ = 0, \quad t_i \notin t_1, t_2, \dots, t_m. \end{aligned} \quad (40)$$

Where  $h_x$  and  $h_y$  is the sampling impulse function of  $X$  and  $Y$  signal, respectively. Moreover,  $a_n$  and  $t_m$  is the last sample time instance of  $X$  and  $Y$  respectively. Both the impulse function for few samples are shown in the part (a) of the Figure 18.

Both the signals are constructed as follows

$$\begin{aligned} X_{a_i} &= w_{X,a_i} \\ Y_{t_j} &= 1.3395 * Y_{t_{j-1}} - 0.9025 * Y_{t_{j-2}} + 0.1 * Y_{t_{j-3}} + C * X_{a_{i-2}} + w_{Y,t_j} \\ &a_{i-2} < a_{i-1} < t_j. \end{aligned} \quad (41)$$

Where  $X_{a_i}$  and  $Y_{t_j}$  is the value of the signal  $X$  and  $Y$  at the time instance  $a_i$  and  $t_j$  respectively. And  $w_{X,a_i}$  and  $w_{Y,t_j}$  are random independent IID processes that are Gaussian distributed. Finally,  $C$  is the coupling constant that is linearly varied from 0 to 1 in the steps of 0.01 to increase the coupling strength from  $X$  to  $Y$ . The few samples of both the signal is shown in the (b) part of the Figure 18. The high frequent signal  $Y$  is downsampled to  $X$  frequency by computing the average of  $Y$  instances between the two  $X$  instances. The few samples of original signal  $X$  and downsampled signal  $Y$  are shown in the (c) part of the Figure 18.

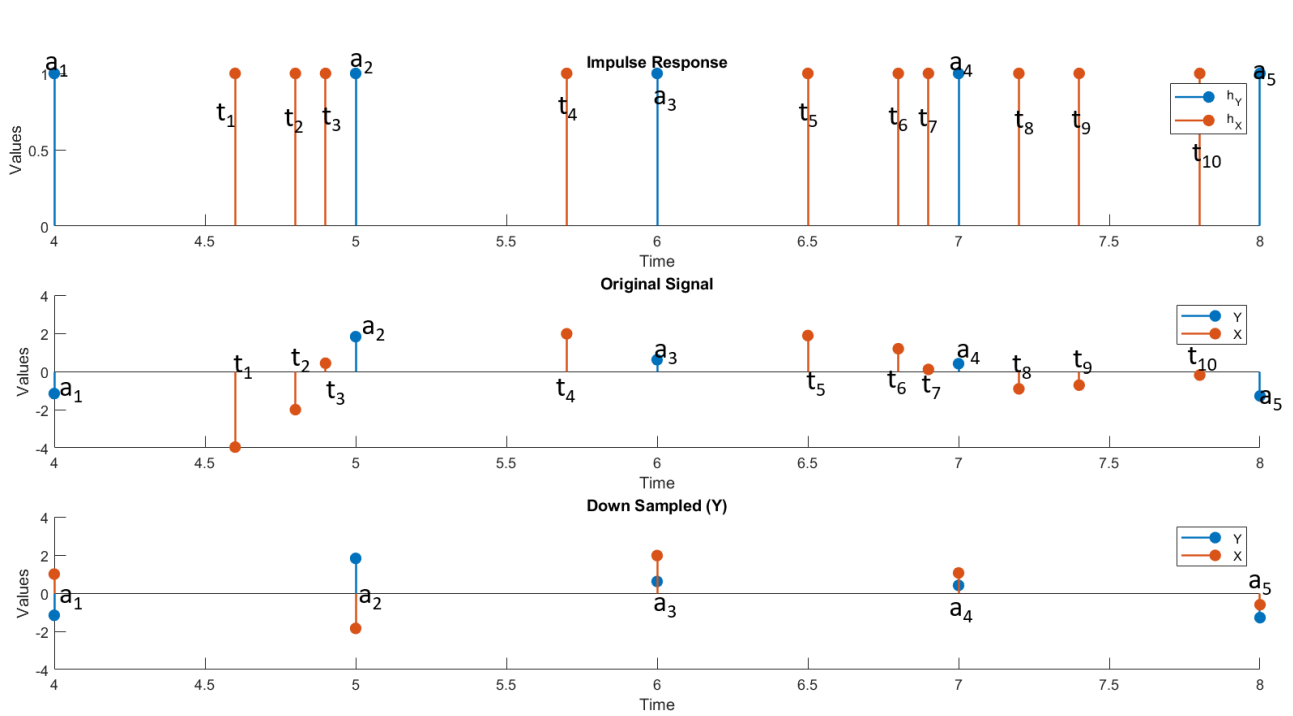


Figure 18: The impulse sampling function of  $h_X$  and  $h_Y$  (a), original signal  $X$  and  $Y$  (b), and down sampled signal  $Y$  (c) are depicted in the figure.

The method explained in section 3.7 and section 3.2 is used to calculate the Granger Causality from  $X \rightarrow Y$  for the unequal sampled case (part b of Figure 18) and equal sampled case (part c of Figure 18) respectively. The Granger causality values for both the cases are calculated for different values of  $C$  that are linearly varied from 0 to 1 in the steps of 0.01. The solid red and solid blue line represents GC for the original and down-sampled signal respectively in the Figure 19. The experiment is repeated 100 times and the variations between the 25th and 75th percentile are depicted in the same Figure 19.

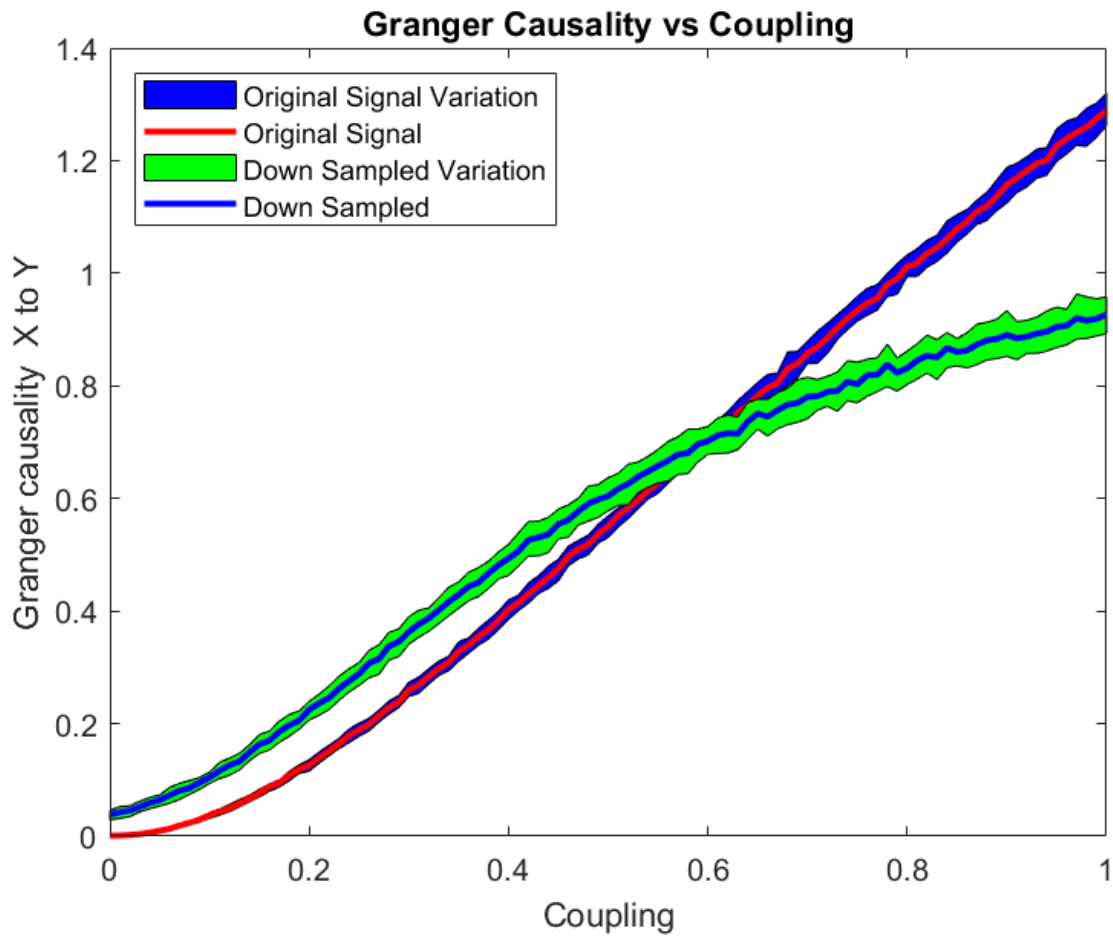


Figure 19: The Granger Causality of  $X \rightarrow Y$  evaluated by two different methods is plotted for different values of coupling strength  $C$ .

The GC calculated on downsampled signal is overestimating initially, while the GC value in the case of the original signal starts with zero. Both approaches can capture the trend. That is, as the coupling strength increases, the GC value from  $X \rightarrow Y$  also increases. We used the uneven Granger Causality method to find the coupling between the respiration and ECG parameters because it is more fundamental and takes no assumptions.

### 3 Methodology of Evaluating Coupling in Real Data

In this chapter, we discuss how the methods of chapter 2 are applied in the real dataset. In section 3.1 given dataset is discussed. In section 3.2 and section 3.3, necessary preprocessing steps are applied to remove the outliers missing values and baseline wandering . In section 3.4, whole pipeline of calculating GC value from the given dataset is presented.

#### 3.1 Dataset

We have four types of datasets obtained from guinea pigs. The first and second dataset was obtained in animals intravenously and subcutaneous exposed to fentanyl, respectively. The dose was variable across animals and ranged from 0.4 to 32mg/kg. The third and fourth dataset was obtained in animals percutaneously exposed to VX. The dose was set at 1 mg/kg and 2mg/kg in third ad fourth dataset, respectively. Overview of the dataset is shown in table-1 where negative control represents the number of animals with 0mg/kg dosage.

Table 1: Different types of exposure with total number of animals

Type of Dataset	Total Number of animals	Negative Control	Dosage
Fentanyl intravenous exposure	26	6	0 – 16 mg/kg
Fentanyl subcutaneous exposure	45	6	0 – 32 mg/kg
VX Percutaan classificatie	32	0	1mg/kg
VX Percutaneous RSDL	32	0	2mg/kg

The brief description of each of the ECG derived parameters are given below and its pictorial representation is shown in Figure 20.

- RR Interval ( $RR_I$ ) : The time difference in milliseconds from one R peak to the next R peak.
- ST Elevation( $ST_E$ ) : The height of ST segment in millivolts from the iso electric line [49].
- QRS duration : The time interval of QRS wave in milliseconds, from Q wave to the S wave.
- R wave height ( $R_h$ ) : The height of R wave in millivolts from the iso-electric level.

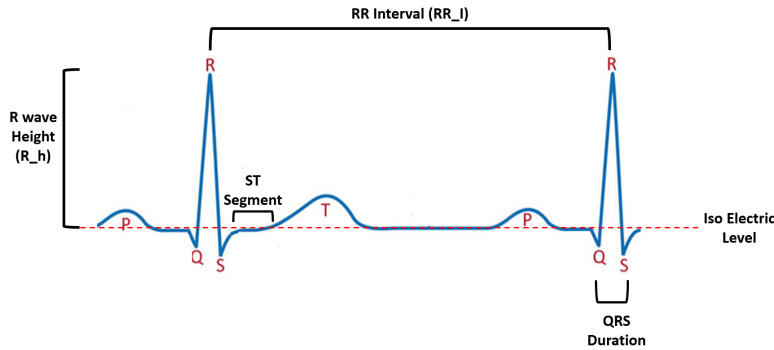


Figure 20: Different features of ECG signal considered in this thesis [57].

The brief description of each of the respiration derived parameters are given below and its pictorial representation is shown in Figure 21,

- Inspiration Time (IT) : The time difference in milliseconds from the start of the inspiration to the end of inspiration. Or the total time of inhalation. The start point of the inspiration cycle is where the respiration signal crosses the baseline with a positive slope. Similarly, the endpoint of the inspiration cycle is where the respiration signal crosses the baseline with a negative slope.
- Expiration Time (IT) : The time interval in milliseconds from the end of the inspiration to the end of expiration.Or the total time of exhalation. The endpoint of the expiration cycle is where the respiration signal crosses the baseline with a positive slope.

- Peak Inspiration Flow (PIF): The highest rate of inhalation in the particular cycle of inspiration. It is the highest point from the baseline. The baseline is defined as the line formed by connecting the start point of the inspiration and the start point of the expiration.
- Peak Expiration Flow (PEF): The highest rate of exhalation in the particular cycle of expiration. It is the lowest point measured from the baseline.
- Total Volume (TV) : It is an area between the inspiration curve and the baseline. Or the total volume of air inhaled in one complete cycle of breathing.

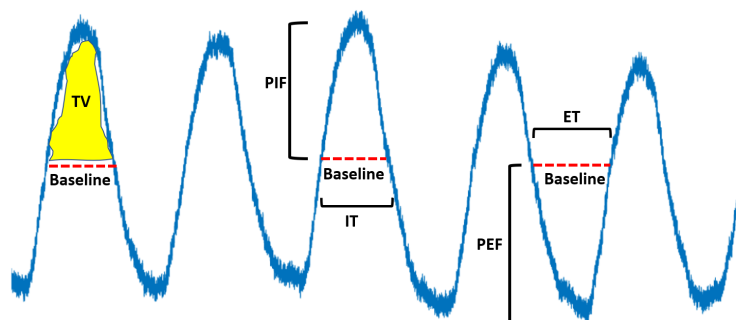


Figure 21: Different features of breathing signal [43]

Fentanyl exposure causes dose-dependent depression in respiration signal [47], an overdose of it causes bradycardia and loss of consciousness/ coma [25]. Therefore, after the exposure heart rate, PIF, PEF and MV are expected to decrease. For few animals, PIF and heart rate deviation from healthy baseline after the exposure to the VX chemical are shown in Figure 22. According to the figure, after the exposure there is more drop in the PIF (breathing parameter) than the heart rate (an ECG parameter).

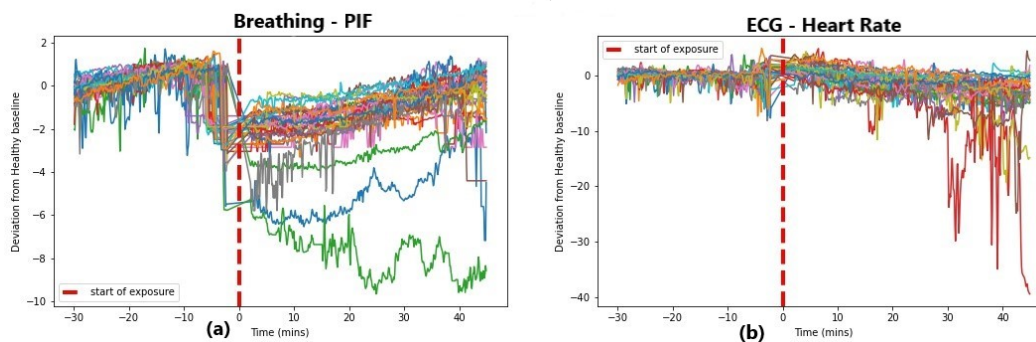


Figure 22: (a) PIF and (b) heart rate deviation from healthy baseline after the exposure to the VX chemical. Different animals' signal are encoded with different colours. After the exposure there is more drop in the PIF (a breathing parameter) than the heart rate (an ECG parameter).

Vx chemical is a type of organophosphates whose exposure causes bradycardia [11], failure of respiration system [7] and its prolonged exposure can cause ataxia [8]. Therefore, after the exposure heart rate, PIF, PEF and MV are expected to decrease. Whereas in EEG, the power of the low-frequency component might increase after prolonged exposure. In this thesis we worked on ECG and breathing parameters.

### 3.2 Preprocessing

The missing values are imputed using spline interpolation [66][13]. After imputing the missing values, the outlier detection is performed using moving median absolute deviation method [41][67]. Outliers are characterized as points more than three times MAD from the median over the windows of 300 samples. The MAD is denoted as

$$\begin{aligned}
MAD &= c * \text{median}(\|A - \text{median}(A)\|_1) \\
c &= \frac{-1}{\sqrt{2} * \text{erfcinv}(3/2)} \\
\text{erfc}(x) &= \frac{2 * \int_x^\infty e^{-t^2} dt}{\sqrt{\pi}} \\
\text{erfcinv}(y) &= \text{inverse}(\text{erfc}(x)) \quad , \text{ where } y = \text{erfc}(x)
\end{aligned} \tag{42}$$

Detected outlier points are imputed using spline interpolation. Finally, the baseline correction is done using an 8-level maximal overlap discrete wavelet transform (MODWT) with a symlet wavelet with four vanishing moments [64][63]. We did the baseline correction to make the signal approximately stationary over the shorter windows. A detailed explanation is in the method section. The decomposition of each level of the transformation will result in 8 detail signals and one approximation signal (or baseline). The approximation signal is subtracted from the original signal to evaluate the baseline-corrected signal (or transformed signal). The Figure 23 shows the baseline line correction using MODWT-8 of the PIF signal of one of the animals. The increase in the levels will create a smoother baseline that fails to detect the actual trends. The decrease in the levels can cause the removal of useful information in the form of sharp transactions. Zitong Zhang et.al, discussed the benefit of using MODWT over DWT (Discrete wavelet transform) with the proper choice of wavelet [52].

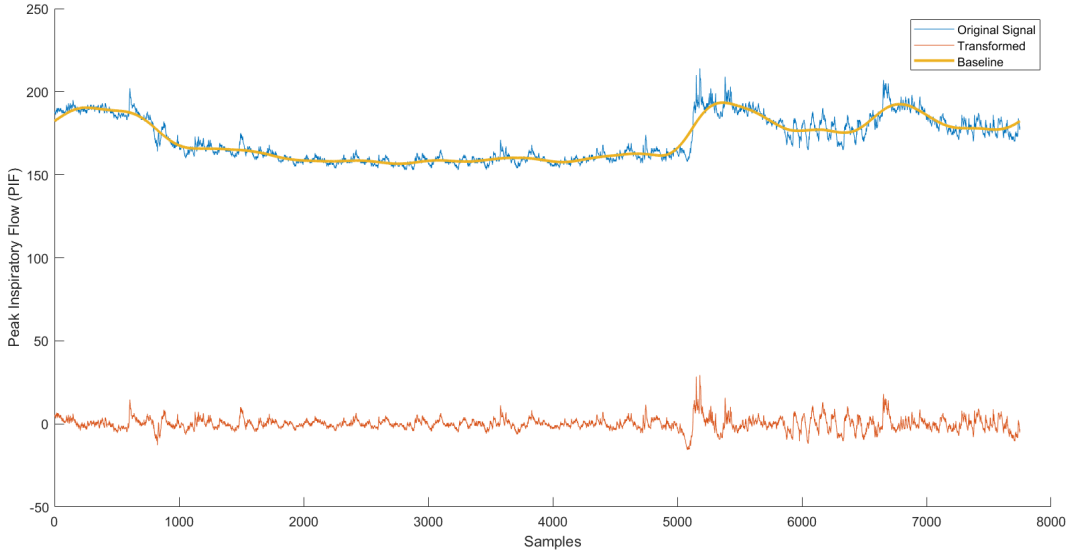


Figure 23: Baseline correction of the original signal (blue line) using Wavelet transform.

### 3.3 Signal Segmentation

The GC assumes the signal to be stationary. For computing the interactions correctly we need to segment our signals into stationary segments and the signals that we have received is non-stationary. But we can bifurcate it into series of successive, same length segments, each with stationary signals properties. Here we aimed to find the stationary segments by combining the smaller segments of fixed length which have same second order statistics.

For comparison, we considered two windows of a fixed length of 50 samples each. We call one reference window and the other one sliding window. The estimate of the signal statistics is obtained from the reference window and compared to the statistics of the sliding test window by a comparing dissimilarity value calculated as

$$\text{Dissimilarity} = \sum_{k=0}^{50} (r_R(k) - r_T(k))^2, \tag{43}$$

where  $r_R(k)$  and  $r_T(k)$  denotes the correlation values at  $k$  lag value of reference and sliding windows, respectively. Other way is to make reference window dynamic size as long as no prominent change is detected and then compare its properties to the sliding window. Both methods are summarized in Figure 24. We have used the first method of fixed reference window and sliding test window. Both of the methods of stationary segmentation are explained by Rangayyan [48].

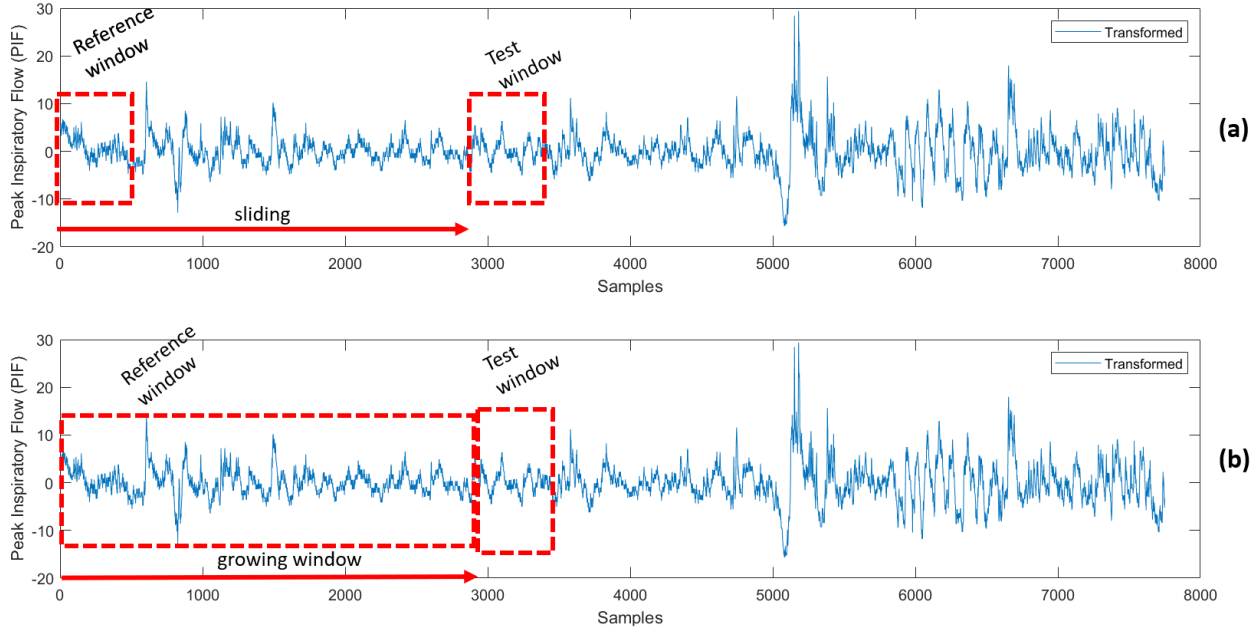


Figure 24: Two different approaches are shown in the figure a) Fixed reference window and b) Growing reference window [48]

We calculated successive dissimilarity (dissimilarity value current window is compared to the previous window) for all the animals and for each feature separately. Whenever there is a sharp transition, it suggests that the current segment and the previous segment have different second order characteristics. The threshold is decided with respect to the stationary Gaussian process whose dissimilarity is also calculated in the same way. Successive dissimilarity of one animal is plotted in Figure 25 and Figure 26, separately for ECG and breathing parameters, respectively.

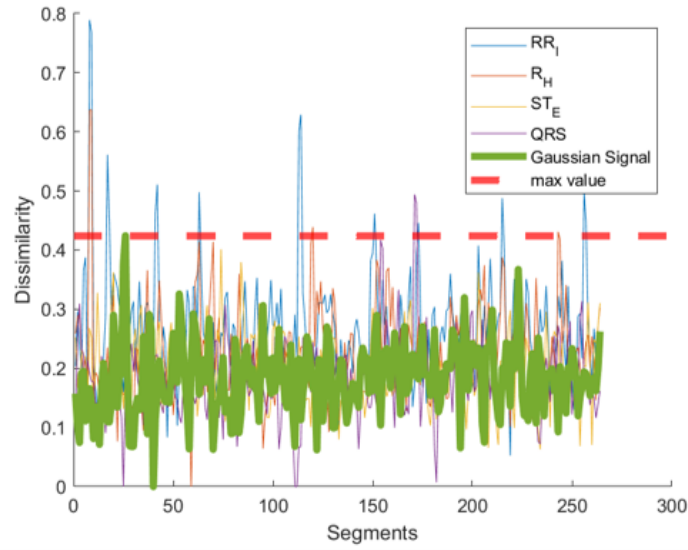


Figure 25: The successive dissimilarity of ECG parameters is plotted. Each number on X-axis denotes the segment of 50 samples each. The thick line is the dissimilarity of the stationary Gaussian process.

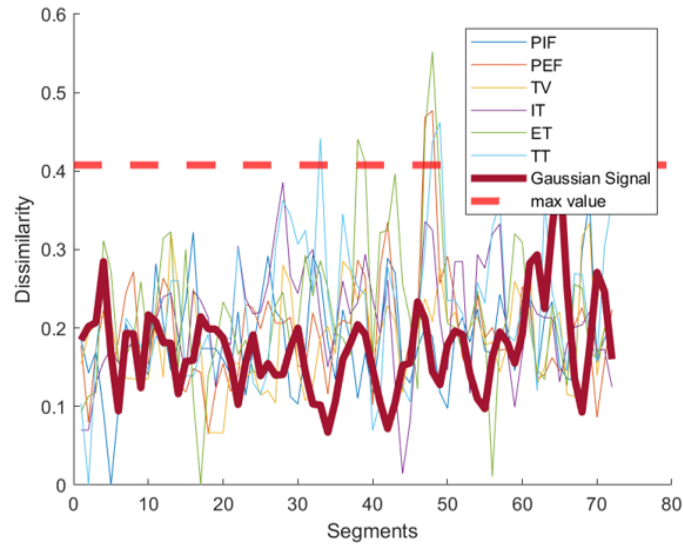


Figure 26: The successive dissimilarity of Breathing parameters is plotted. Each number on X-axis denotes the segment of 50 samples each. The thick line is the dissimilarity of the stationary Gaussian process.

We visualized the above plots for all other animals and concluded that the window size of 600 samples is the best choice to evaluate GC for both ECG and breathing cases.

### 3.4 Experiment Design

In this section we explained how exactly we used previously discussed methods to calculate the GC of the given dataset. In this work we calculated the three types of interactions as follows

- Within ECG parameters
- Within Respiration parameters
- Between Respiration and ECG parameters

The original formulation of GC (section 2.2.1) is used to determine the direct causality in the above first two cases, while we used unequal sampled GC (section 2.1.2) for the last case. First, we imputed the missing values and outliers before doing baseline correction, as described in section 3.2. Then, for the first two cases, we bifurcated the signal into overlapping windows of size 600 samples with 80% overlap. In each window, we evaluated the GC and tested its significance using F tests and surrogate analysis as discussed in the section 2.1.1 and 2.2, respectively. We stacked the obtained GC values vertically in a single matrix to get a Granger causality matrix for each animal. The steps after preprocessing is described in Figure 27. For simplicity, we have depicted the non-overlapping windows in the figure.

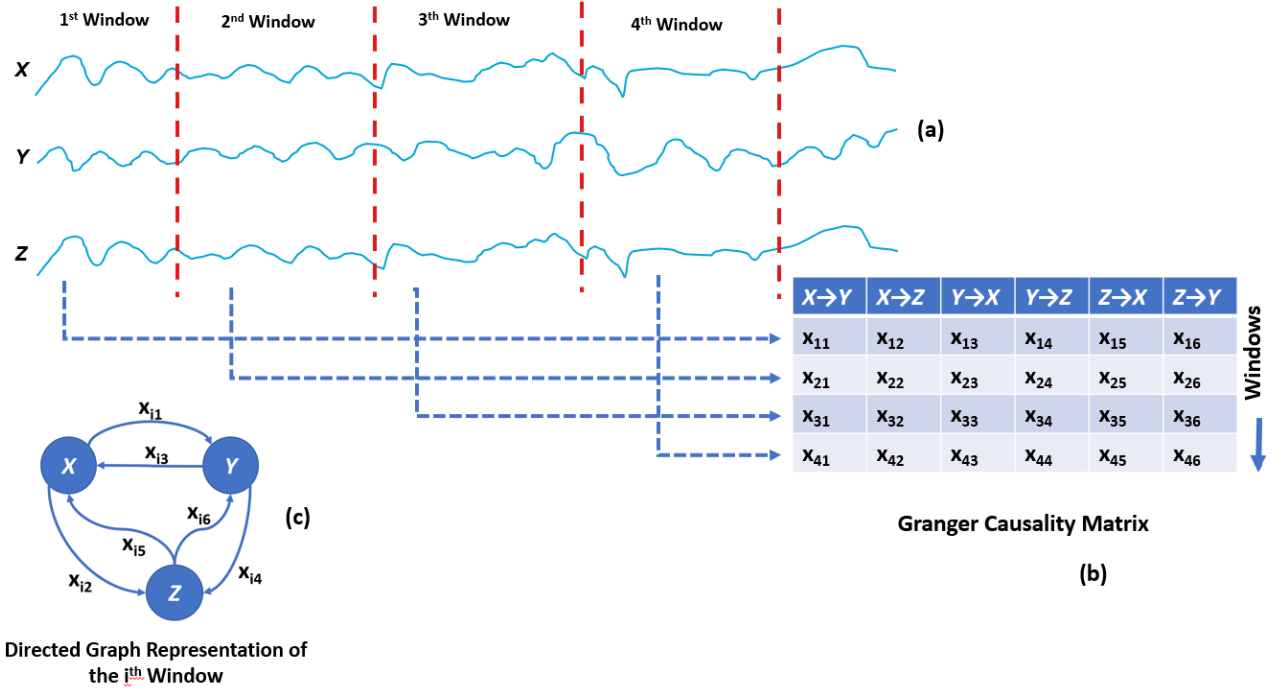


Figure 27: The steps involved after preprocessing to get GC matrix. Let's consider the three variables system ( $X, Y$ , and  $Z$ ) and the signal associated with each variable are already preprocessed and baseline corrected. (a) We first bifurcated the set of signals into overlapping windows of size 600 samples with 80% overlap. We have depicted the non-overlapping windows for simplicity. (b) For each window separately, we evaluated the GC and tested its significance using F tests and surrogate analysis. We vertically stacked the obtained GC values in a matrix to get a Granger causality matrix for each animal. Where the first row signifies the interactions of the first window. And  $x_{i,j}$  is the GC value of  $j^{th}$  link calculated in the  $i^{th}$  window (c) We have represented the  $i^{th}$  window interactions in the form of a directed graph.

For calculating the causality between ECG and respiration parameters, we bifurcated the ECG signal into overlapping windows of size 2000 samples with 80% overlap and considered the respective respiration signal window. We used the unevenly sampled GC method as discussed in section 2.2. to evaluate causalities. Finally, we utilised F-tests and surrogate analysis for significance testing.

## 4 Classification of Granger Causality for exposure detection

In this chapter, interactions features obtained from Chapter 3 are used to develop a prediction model that differentiates between healthy and exposure state and between VX and Fentanyl class of chemicals. The flow chart in Figure 28 depicts modelling steps that we have incorporated.

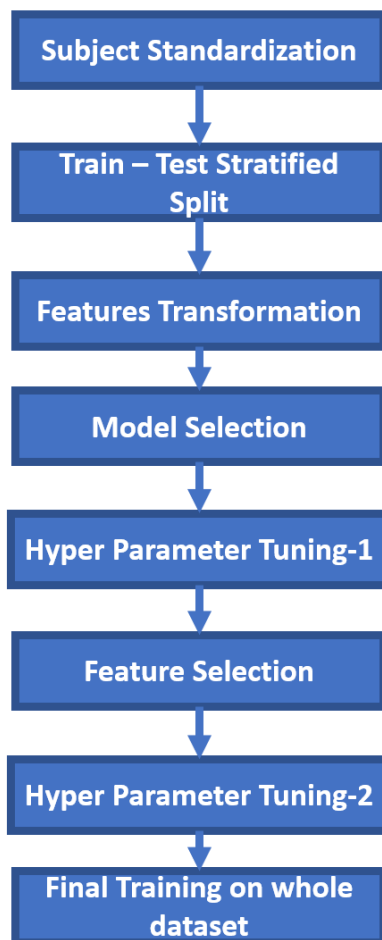


Figure 28: Steps followed for modelling.

### 4.1 Train Test Stratified Splitting

Train test splitting is the procedure to split the dataset into train and test sets. We used the train set to train the model and used the test set to estimate the performance of the trained model. We excluded the test set during the training phase and used it only during the final evaluation of the model.

While splitting, we ensured that the proportion of animals of VX and Fentanyl in both training and testing sets are similar. The Figure 29 shows the number of animals that we have considered for training and testing sets for both ECG parameters and breathing parameters, separately. The proportions of number of animals belonging to each type of chemicals are approximately 0.2 for the test set, and 0.8 for the training set.

### Breathing Parameters

Chemical	Total Animals	Test Animals	Train Animals
VX Chemical	49	11	38 = (31 + <b>7</b> )
Fentanyl Chemical	46	10	35 = (28 + <b>7</b> )
	95	21	73 = (59 + <b>14</b> )

### ECG Parameters

Chemical	Total Animals	Test Animals	Train Animals
VX Chemical	51	11	40 = (32 + <b>8</b> )
Fentanyl Chemical	55	11	44 = (36 + <b>8</b> )
	106	22	84 = (68 + <b>16</b> )

Figure 29: Test -Train -Validation Stratified Split for both ECG parameters and breathing parameters. The red bolded numbers in the table show the number of validation of animals. The proportion of the number of test, train and validation animals is approximately equal in each cases.

For proper evaluation of the model during the training phase, we used the five-fold cross-validation evaluation method. The train set is further splitted into train and validation sets in a stratified fashion on the type of chemicals. In Figure 29, the red font number represents the number of validation animals considered for each cases.

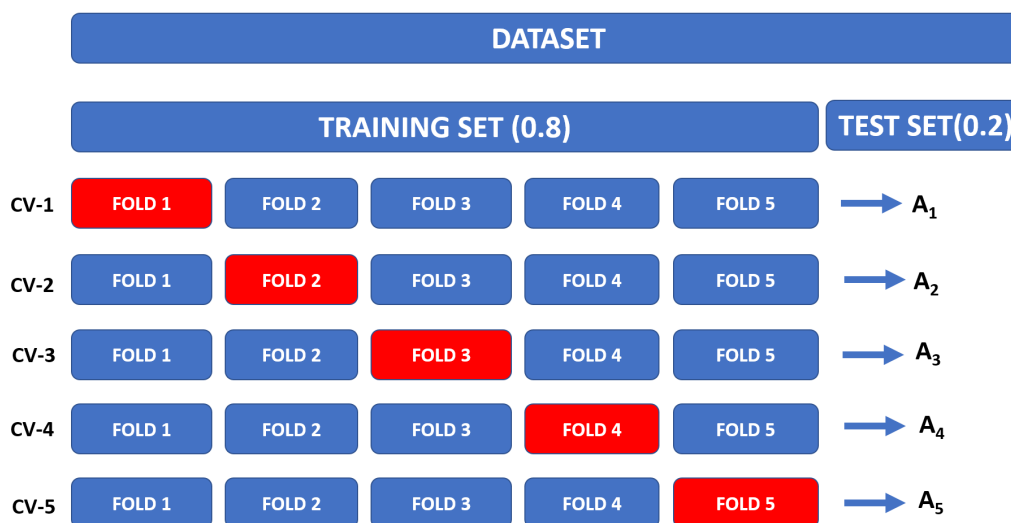


Figure 30: Dataset splitting into train and test sets. We used five-fold cross-validation to evaluate the model performance in the training phase. At each fold, the number of animals is the same and but the animals are different. We used the test set only at the final evaluation of the final model.

For assessing the performance of a model with a definite set of parameters, the training set is splitted into five folds ( Figure 30). Such that the size of all the folds are the same but have different animals. At each iteration of the cross-validation, one fold is used for testing and the remaining folds are used for training. For example, in the first iteration (CV-1) fold-1 is used for testing and fold-2,3,4,5 are used for training. The accuracy obtained during this iteration is denoted as  $A_1$ .

The performance of the model during the training phase is given by the mean ( $\bar{A}$ ) and the standard deviation

( $\sigma_A$ ) of cross-validation accuracies, that are denoted as

$$\begin{aligned}\bar{A} &= \frac{\sum_{k=1}^{k=5} A_i}{5} \\ \sigma_A &= \sqrt{\frac{(A_i - \bar{A})^2}{5}}\end{aligned}\quad (44)$$

where,  $A_i$  is the accuracy of the model at the  $i^{th}$  cross-validation iteration.

## 4.2 Features Scaling

The GC values evaluated for each animal need to be made on the same scale to get the classification model better generalizable among different animals. To achieve this, we used the Standardization scaling (SD) technique. SD centred the feature values around the mean with a unit standard deviation, resulting in zero mean and distribution of unit standard deviation. SD does not have a bounding range, so it is robust to outliers or links that have unusual coupling strength.

The formulation of SD is given as

$$X' = \frac{X - \mu}{\sigma} \quad (45)$$

where  $\mu$  is the mean of the feature values( $X$ ),  $\sigma$  is the standard deviation of the feature values( $X$ ) and  $X'$  is the new scaled feature.

In our case, we standardized each animal separately with their respective healthy part of the evaluated GC mean and standard deviation. Such that the healthy region of all animals have the same mean and unit variance. At the same time, it ensures significant differences between the healthy and exposure regions.

Let's consider two GC matrices X and Y ( Figure 31). Where X is a healthy GC matrix and Y is an exposed GC matrix. Each GC matrix has p columns that denote the p number of links. The rows represent different windows. Healthy GC matrix and exposed GC matrix have n and m total windows, respectively.

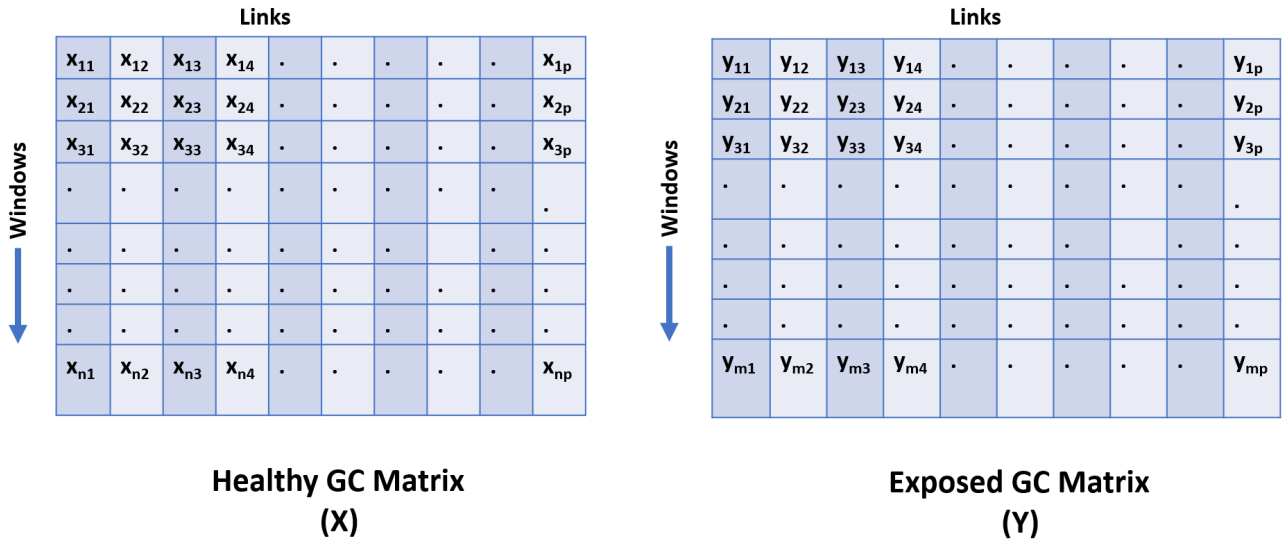


Figure 31: Notation of evaluated GC Matrix and Healthy (X) and Exposure (Y) region of a animal. Where rows and columns represent windows and links, respectively. The healthy GC matrix have p links and n windows, similarly the exposed GC matrix have p links and m windows.

Furthermore,  $\bar{x}_1, \bar{x}_2, \bar{x}_3, \dots, \bar{x}_p$  represent the mean value of 1st link, 2nd Link, 3rd Link and so on, respectively of matrix X (see equation (46)). Similarly  $\sigma_{x_1}, \sigma_{x_2}, \sigma_{x_3}, \dots, \sigma_{x_p}$  represent the standard deviation of 1st link, 2nd Link, 3rd Link and so on, respectively of matrix X (see equation (47)).

$$\bar{x}_k = \frac{\sum_{i=1}^n x_{ik}}{n} , k \in 1, 2, 3, \dots, p . \quad (46)$$

$$\sigma_{x_k} = \sqrt{\frac{\sum_{i=1}^n (x_{ik} - \bar{x}_k)^2}{n}} , k \in 1, 2, 3, \dots, p . \quad (47)$$

Then we applied the standardization equation -(45) to each of the entries of matrix X and Y to get new transformed matrix  $X'$  and  $Y'$  as

$$\begin{aligned} x'_{i,k} &= \frac{x_{i,k} - \bar{x}_k}{\sigma_{x_k}} , k \in 1, 2, 3, \dots, p \\ i &\in 1, 2, 3, \dots, n , \end{aligned} \quad (48)$$

and

$$\begin{aligned} y'_{i,k} &= \frac{y_{i,k} - \bar{y}_k}{\sigma_{y_k}} , k \in 1, 2, 3, \dots, p \\ i &\in 1, 2, 3, \dots, m . \end{aligned} \quad (49)$$

Where  $x'_{i,k}$  and  $y'_{i,k}$  are the entries of the transformed matrix  $X'$  and  $Y'$ , respectively.

### 4.3 Principal Component Analysis

Principle Component Analysis (PCA) [44] is an unsupervised learning technique for extracting hidden structures from high dimensional datasets. We have 12 and 20 interactions features from ECG and breathing derived parameters, respectively. To properly train the classification model on fewer subjects, we need to make the features much more informative. So, we intend to find the common subspace on which the GC features of the healthy region of all the animals have the highest variance.

Suppose we have a data Matrix  $X^{n \times p}$ , where n is the total number of entries and p is the number of features. Then the covariance matrix of X is given by

$$\Sigma^{p \times p} = \frac{X^T * X}{n} , \text{ where X is already centered ,} \quad (50)$$

Furthermore, the eigenvalue and eigenvector of covarinance matrix  $\Sigma$  are related as

$$\Sigma^{p \times p} = U * \Lambda * U^T , \quad (51)$$

Where  $U$  and  $\Lambda$  are the eigenvector and eigenvalue matrices of  $\Sigma$ , respectively. The eigenvector corresponding to the largest eigenvalue is called the first principal component, this component corresponds to the direction with the most variance. We get p eigenvectors corresponding to each of p eigenvalues after solving the equation (51). The data matrix (X) can be transformed into a more informative matrix by projecting it into the subspace of eigenvectors. The new data matrix  $\hat{X}$  is denoted as

$$\hat{X} = X * U \quad (52)$$

Apart from transformation, another main use case of PCA is to reduce the dimension of the dataset. Ian Jolliffe Analysis [22] suggested multiple methods to achieve feature reduction using PCA in his paper. We have used the Scree test [2] or elbow method to visualize the importance of eigenvalues.

As described above, we are interested in finding the common subspace concerning the healthy region by considering all the subjects. So we created a new data matrix by stacking the healthy part of computed GC matrices of all the subjects into one single large matrix, denoted as

$$X_{healthy} = \begin{bmatrix} X_1^{n_1 p} \\ X_1^{n_2 p} \\ X_1^{n_3 p} \\ X_1^{n_4 p} \\ \dots \\ X_k^{n_k p} \end{bmatrix} \quad (53)$$

Where  $X_k^{n_k p}$  denotes the  $k_{th}$  subject healthy GC matrix with  $n_k$  entries and  $p$  links. Then we calculated the covariance matrix ( $\Sigma_{healthy}$ ) of  $X_{healthy}$  by using the equation (50). We computed the eigenvector ( $U_{healthy}$ ) and eigenvalues ( $\Lambda_{healthy}$ ) of covariance matrix by satisfying the equation (51). We plotted the eigen values of ( $\Lambda_{ECG_{healthy}}$ ) and ( $\Lambda_{breathing_{healthy}}$ ) in decreasing order in Figure 32 for checking the importance of eigenvalues or for any scope of dimensionality reduction.

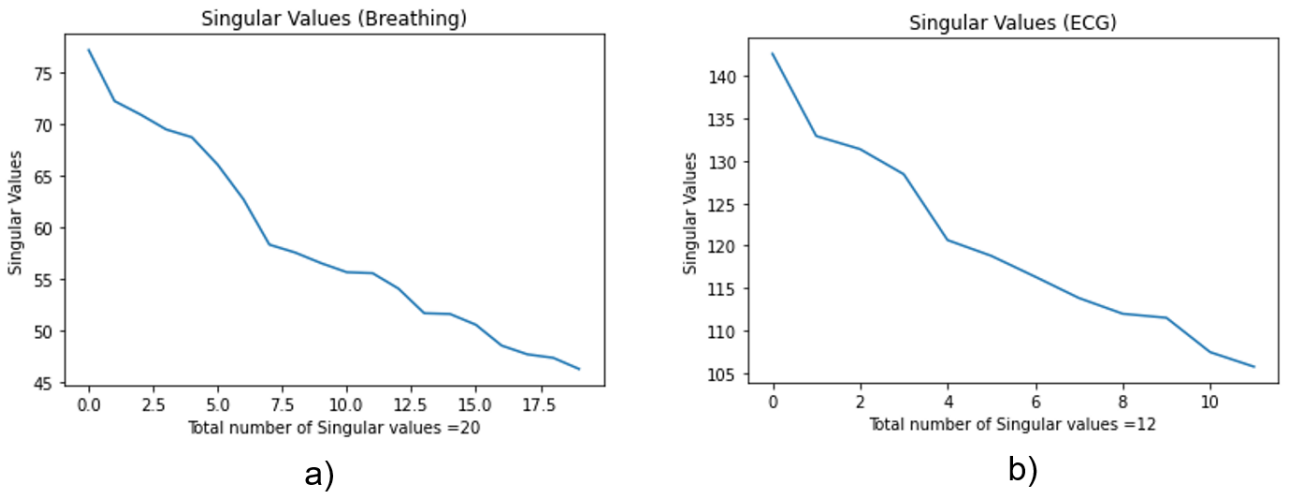


Figure 32: Plot of eigenvalues or singular values in decreasing order for healthy breathing interactions ( $\Lambda_{breathing_{healthy}}$ ) (a) and healthy ECG interactions ( $\Lambda_{ECG_{healthy}}$ ) (b) separately. No significant elbow is there in both plots.

From the above plot, we could not locate the elbow in both the cases, the point where the plot turns from a steep to a flat line. Therefore, we regarded all principal components as important. We used computed eigenvector ( $U_{healthy}$ ) to project the exposure part of the subjects into a healthy subspace. Though we have not achieved the dimensional reduction through PCA, we have projected (or transformed) our feature to a more informative subspace, that will aid in better performance of the model.

#### 4.4 Model Selection

Model selection is a process of selecting the machine learning model from the collection of possible models based on the training set. We trained nine different classification algorithms, each with the default scikit-learn parameters [39] and evaluated each of them using the cross-validation technique.

The nine different classification algorithms that are considered are:

- Random Forest [18]
- Support Vector Machine [15]
  - Radial Basis Kernel (RBF)
  - Polynomial Kernel
  - Linear Kernel

- K Neighbours Classifier [9]
- Decision Tree [40]
- Naïve Bayes [21]
- Linear Discriminant Analysis [50]
- Logistic Regression [50]

For each of the above algorithms, we evaluated the model performance on the mean and standard deviation of cross-validations accuracies for two-way classification (Figure 33) and three-way classification (Figure 34) problem. Where the two-way classification model differentiates the samples between healthy and exposure. And, three-way classification discriminates between healthy, VX and Fentanyl.

Model	Breathing Parameters	ECG Parameters
<b>Random Forest</b>	77.56% +/- 3.37%	64.27% +/- 1.97%
<b>Support Vector Machine ("RBF")</b>	79.21% +/- 2.94%	65.36% +/- 2.77%
Support Vector Machine ("Linear")	65.67% +/- 3.98%	59.88% +/- 2.54%
Support Vector Machine ("Poly")	70.12% +/- 2.68%	61.76% +/- 3.06%
K Neighbors Classifier	72.41 % +/- 3.76%	60.63% +/- 1.81%
Decision Tree	68.36% +/- 2.21%	57.49% +/- 0.81%
Naïve Bayes	66.88% +/- 2%	62.22% +/- 1.81 %
Linear Discriminant Analysis	65 % +/- 3.91%	59.02% +/- 1.63%
Logistic Regression	64.85% +/- 4.01%	58.58% +/- 1.37%

Figure 33: The table shows the mean and standard deviation cross-validation accuracies for different classification algorithms for the model that differentiate between healthy and exposure. The Random Forest and SVM("RBF") perform best on the training datasets. In all cases, the model based on breathing interactions performs better than the model based on ECG interactions.

Model	Breathing Parameters	ECG Parameters
Random Forest	70.30% +/- 5.12 %	60.71% +/- 1.43%
Support Vector Machine ("RBF")	72.06% +/- 4.43%	60.61% +/- 1.64%
Support Vector Machine ("Linear")	65.36 % +/- 4.46 %	58.16% +/- 2.59%
Support Vector Machine ("Poly")	66.97% +/- 3.53%	58.38% +/- 1.91%
K Neighbours Classifier	65.88% +/- 2.86 %	56.38 +/- 1.4%
Decision Tree	58.77% +/- 3.95%	50.79 +/- 0.9%
Naïve Bayes	61.96% +/- 3.82%	57.63 +/- 1.83%
Linear Discriminant Analysis	63.86% +/- 4.46%	58.58% +/- 1.6%
Logistic Regression	65.69% +/- 3.81%	58.52% +/- 1.67%

Figure 34: The table shows the mean and standard deviation cross-validation accuracies for different classification algorithms for the model that differentiate between healthy, VX and Fentanyl. The Random Forest and SVM("RBF") perform best on the training datasets. In all cases, the model based on breathing interactions performs better than the model based on ECG interactions.

According to the table in the Figure 33 and Figure 34, the Random Forest and SVM("RBF") performed the best on the training datasets. In all cases, the model based on breathing interactions performs better than the model based on ECG interactions. Moreover, in both models the SVM ("RBF") performs better than random forest.

Therefore, we have used the Random forest and support vector machine with radial basis function classifier to classify between normal and exposure using GC as a feature vector.

#### 4.5 Feature Selection

We have used wrapper based methods for feature selection. In wrapper methods, we use a subset of features to train a model. Then we compare the outcome of the current model to the previous one. If the difference is significant, then we decide to add or remove the feature. The procedure of the method is summarized pictorially in the Figure 35.

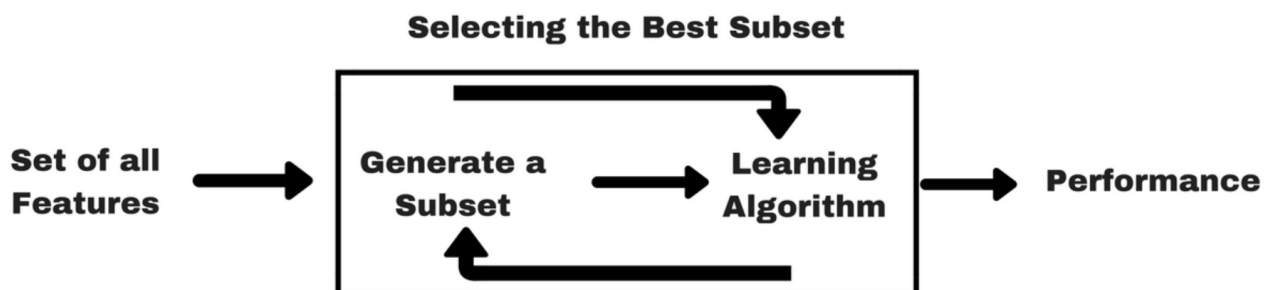


Figure 35: Wrapper Method for Feature selection

Some common technique of wrapper methods are:

- Forward Selection: It is an iterative method in which we start with no features in the model. In every successive iteration, we keep on adding the feature that results in a maximum increase in accuracy.

- **Backward Elimination:** It is an iterative method in which we start with all the features in the model. In every successive iteration, we keep on removing the feature that results in a maximum increase in accuracy. We continue this until no further improvement is observed by removing the features. Backward selection tends to choose a higher dimensional model as compared to the forward selection model.
- **Recursive Feature elimination:** It is a greedy algorithm where we check the model performance for every possible combination of the feature set. This method will result in an optimal solution but it is very computationally expensive.

In this work, we have used the forward selection method to shortlist the features. The feature selection algorithm was implemented for two different models (random forest and SVM), separately for ECG based features set and breathing based features set. We used a five-fold cross-validation method to assess the performance of the model and selected the one with the lowest complexity among the best performing models in each case.

The different scenarios are summarized for the 2 way classification model ( refer Figure 36 ) :

- **Support Vector Machine**
  - ECG parameters: 11 principal components are selected out of 12. They are 1, 12, 7, 5, 9 , 6, 4, 3, 10, 11 and 8 PCs, respectively. ( part (c) of Figure 36 )
  - Breathing parameters: 19 principal components are selected out of 20. They are 1, 11, 10, 6, 20, 12, 3, 17, 4, 15, 9, 5, 2, 7, 14, 8, 18, 19 and 13 PCs, respectively. ( part (d) of Figure 36 )
- **Random Forest Classifier**
  - ECG parameters: 8 principal components are selected out of 12. They are 1, 4, 3, 12, 5 ,7 ,10 and 11 PCs, respectively. ( part (a) of Figure 36 )
  - Breathing parameters: 13 principal components are selected out of 20. They are 3, 1, 4 , 5, 14, 11, 16, 12, 15, 9, 19, 20 and 18 PCs, respectively. ( part (b) of Figure 36 )

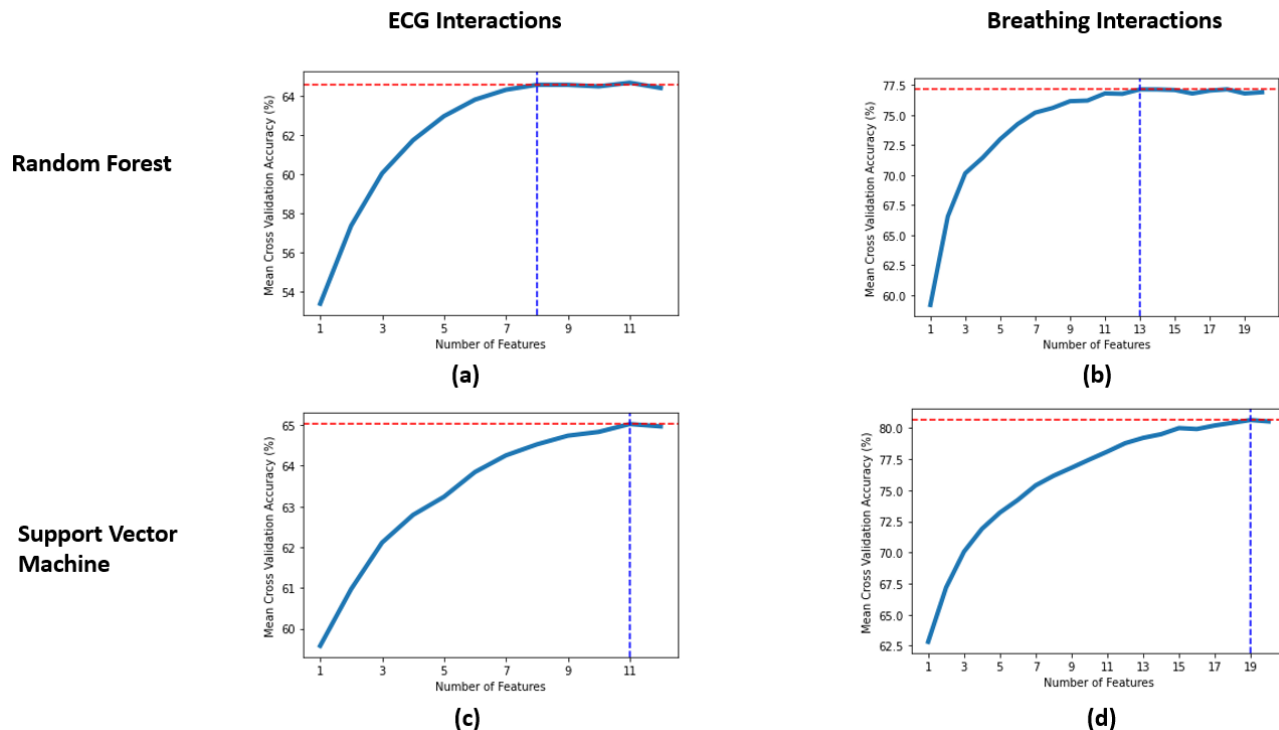


Figure 36: Forward feature selection (FS) results for 2 way classification model are shown. The row index represents the type of model use and the column index indicates the type of features. In each plot, the y axis is the mean cross validation accuracy (MCVA) and x axis is the number of features used. a) Result of FS of random forest trained on ECG based interactions b) Result of FS of random forest trained on respiration based interactions c) Result of FS of SVM trained on ECG based interactions b) Result of FS of SVM trained on respiration based interactions

The different scenarios are summarized for the 3 way classification model (refer Figure 37):

- Support Vector Machine
  - ECG parameters: 11 principal components are selected out of 12. They are 0, 4, 11, 1, 10, 6, 5, 2, 3, 9, 8, and 7 PCs, respectively. ( part (c) of Figure 37 )
  - Breathing parameters: 19 principal components are selected out of 20. They are 20, 3, 1, 9, 11, 5, 12, 13, 10, 2, 17, 6, 4, 14, 19, 16, 18, 8, 7 PCs, respectively. ( part (d) of Figure 37 )
- Random Forest Classifier
  - ECG parameters: 8 principal components are selected out of 12. They are 1, 5, 12, 3, 10, 4, 11 and 7 PCs, respectively. ( part (a) of Figure 37 )
  - Breathing parameters: 12 principal components are selected out of 20. They are 3, 1, 20, 8, 11, 12, 16, 2, 9, 4, 17 and 5 PCs, respectively. ( part (b) of Figure 37 )

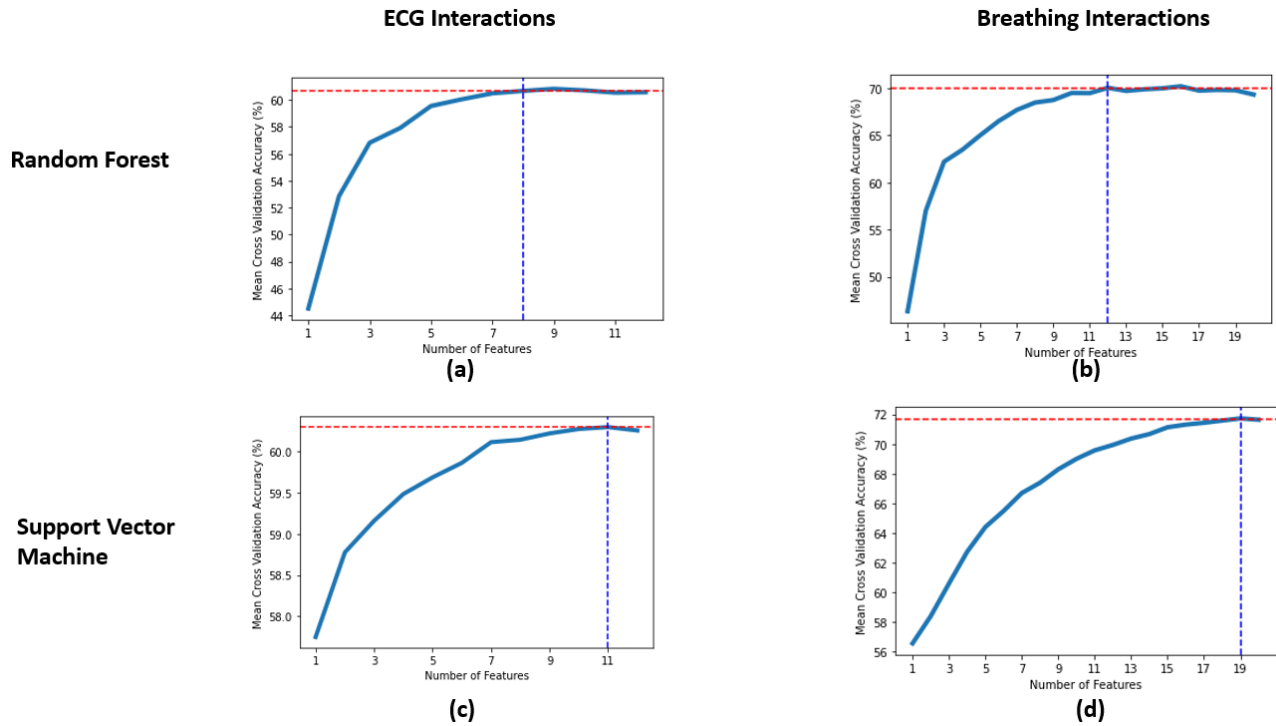


Figure 37: Forward feature selection (FS) results for 3 way classification model are shown. The row index represents the type of model use and the column index indicates the type of features. In each plot, the y axis is the mean cross validation accuracy (MCVA) and x axis is the number of features used. a) Result of FS of random forest trained on ECG based interactions b) Result of FS of random forest trained on respiration based interactions c) Result of FS of SVM trained on ECG based interactions b) Result of FS of SVM trained on respiration based interactions

The feature forward selection of random forest resulted in a simpler model than one with SVM in all of the above cases. Further, the SVM considers almost the whole of the subspace as important for the classification. After the feature selection, we again did the hyperparameter tuning with the reduced set of features.

## 4.6 Implemented Models

### 4.6.1 Random Forest

**Hyper Parameters** Random Forest have several parameters, some important ones are

- Criterion : The function that measures the quality of a split. Ginni impurity and entropy impurity are the two measures. Most of the time, the choice of criterion does not make a big difference. Ginni impurity tends to be faster than entropy impurity. In general, Ginni impurity isolates the most occurring

instances in its branch while the entropy impurity tends to generate a more balanced tree. Because of the computational reason we used Ginni impurity.

- max depth : It controls the maximum depth of the tree. Reducing the max depth will regularize the model and thus reduce the risk of overfitting.
- minimum samples leaf : It expresses the minimum number of samples required at a leaf node. If the available samples are below the specified minimum samples leaf, then the splitting of that leaf won't happen. Increasing the minimum samples leaf will regularize the model and thus reduce the risk of overfitting.
- maximum leaf node : It indicates the maximum leaf nodes in a tree. Reducing the maximum leaf node will regularize the model and thus reduce the risk of overfitting.
- maximum features: It is a number of features to consider when searching for the best split. By default, the model searches for all the features that can result in overfitting.
- bootstrap : It controls whether to use whole sample set to train each tree or use random sampling with replacement.
- number of trees: In general, each individual tree has a higher bias, after including more trees in bagging fashion the bias and variance will reduce. But including more trees into model can over fit the training data.

**Hyper Parameters Tuning:** In this section, we devise a plan to optimally search for the best set parameters that result in the best model. In this work, we implemented two times hyperparameter tuning, one before and after the feature forward selection. At each time, we evaluated a different combination of parameters and, the set of parameters with the highest cross-validation accuracy is selected. The final set of tune hyper parameters for each case is shown in the Figure 38.

Parameters	Exposure Vs Heathy		Healthy vs VX vs Fentanyl	
	Breathing	ECG	Breathing	ECG
Number of Trees	100	100	100	100
Min Samples Split	20	2	2	2
Min Samples Leaf	2	1	1	1
Max Features	4	3	3	3
Max Depth	60	Until all leaves are pure	Until all leaves are pure	Until all leaves are pure
Bootstrap	True	True	True	True

Figure 38: The sets of tuned hyperparameters of random forests after the feature forward selection for each case.

#### 4.6.2 Support Vector Machine

**Hyper Parameters:** Support vector machine with radial basis function have two major hyper parameters that are

- gamma : It is a scaling factor in the radial basis function. As gamma increases, the influence of an instance on other instances reduces or the effect of an instance become much more localized. A higher value of gamma results in sharp or irregular decision boundaries. Conversely, a smaller gamma results in more influence of an instance to other instances creating a much smoother or regular decision boundary. So gamma acts like a regularization hyperparameter, where higher value tends to overfit the training data and lower values can create underfit model.
- C : The main goal of the SVM classifier is to have a well balanced flexible margin with fewer instances violations. The C interplays between the soft and hard margin classification. Where strict hard margin classifier does not allow any instances to be at the wrong side of the decision boundary. Conversely, the soft margin classifier allows for fewer wrong classifications. The model with a large C tends to be a hard margin classifier. Therefore if the model is overfitting, then we should regularize the model by reducing C.

**Hyper Parameters Tuning** In this section, we devise a plan to optimally search for the best set of parameters for SVM. In this work, we implemented two times hyperparameter tuning. One before and after the feature forward selection. At each time, we evaluate a different combination of parameters and, the set of parameters with the highest cross-validation accuracy is selected. The following strategy is employed for the hyperparameter tuning of the hyperparameters of the support vector machine with radial basis function.

The different combinations of C and gamma are taken as follows

- $C \in [10^{-6}, 10^6]$  with the step size of 10
- $\gamma \in [10^{-6}, 10^6]$  with the step size of 10

If the optimal parameter set lie at the boundary then the maximum or minimum range is increased or decreased respectively. An example of grid search is shown in Figure 39, in the form of heat map for one of the above case.

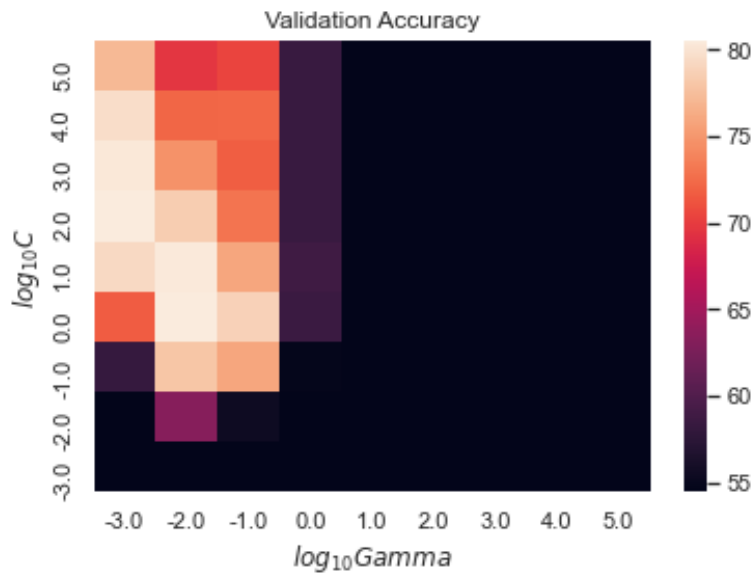


Figure 39: Grid Search of optimal parameters of C and gamma.(Breathing parameters)

The final set of tune hyper parameters for each case is shown in Figure 40.

Parameters	Exposure Vs Heathy		Healthy vs VX vs Fentanyl	
	Breathing	ECG	Breathing	ECG
C	1	10	1	1
Gamma	0.01	0.1	0.01	0.001

Figure 40: The sets of tuned hyperparameters of SVM after the feature forward selection for each case.

## 5 Result

In this chapter, we analysed the causality result of chapter 3 and tested the train model performance on the independent test set. In section 5.1, we used weighted graph density to analyse the strength of the coupling before and after the exposure. In section 5.2, we first defined the evaluation metrics and then discussed the model performance on an independent test set.

### 5.1 Interactions Analysis

In this section, we investigated how the strength of the interactions changes after the exposure to VX or Fentanyl chemicals.

#### 5.1.1 Weighted Graph Density

We can express each row of the GC matrix as a directed graph (see for an example Figure 41). Therefore, number of graph metrics could be used to get the key insights into how the interactions between the parameters are changing [35] and how it alters certain graph properties. Directed graphs mostly have an unsymmetrical matrix that results in complex eigenvalues [60]. Therefore most of the undirected graph metrics [35][23] can't be used in directed GC network for investigation. In this work, we used weighted graph density to measure the cumulative strength of a GC network.

Let's consider a Granger Causality (GC) Matrix for three parameter case ( $p_1, p_2, p_3$ ) as denoted in Figure 41. Where each row represents a window in which GC values are evaluated and columns denote different links. For example the first column of the matrix denotes the link from  $p_1$  to  $p_2$  and similarly, last column of the matrix denotes the link from  $p_2$  to  $p_3$ . Each cell of the matrix ( $x_{ik}$ ) expresses GC value that is calculated for  $k^{th}$  link in the  $i^{th}$  window.

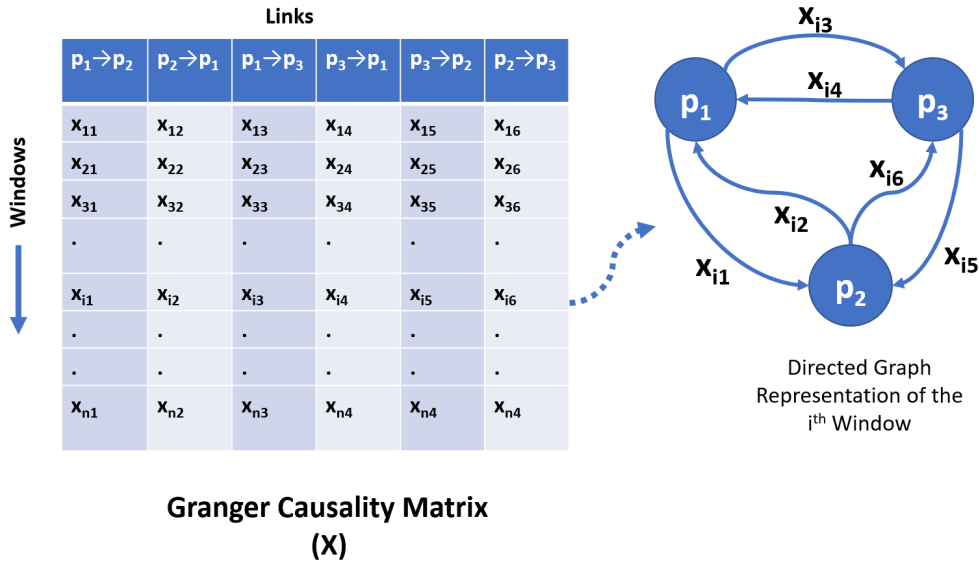


Figure 41: Representation of a Granger Causality matrix row into directed graph.

Each  $i^{th}$  window of the GC matrix can be represented as a directed weighted graph as shown in the above figure. Moreover, we evaluated weighted graph density ( $GD_i$ ) of a directed graph at a  $i^{th}$  window as

$$GD_i = \frac{\sum_{j=1}^p x_{i,j}}{p}, \quad p \in \text{total number of links} \quad (54)$$

The high  $GD_i$  value implies well strongly connected graph. That is, there are a lot of strong interactions between the parameters. Furthermore, we calculated the average graph density (GD) for the same condition (that is healthy or exposure) as

$$GD = \frac{\sum_{i=1}^n GD_i}{n}, \quad n \in \text{total number of windows.} \quad (55)$$

A matrix with a significantly higher GD value has stronger links as against the matrix with a lower GD value.

### 5.1.2 Interactions Insights

In this work we calculated the three types of interactions as follows

- Between ECG parameters
- Between Respiration parameters
- Between Respiration and ECG parameters

In general, most animals have the following links common in their healthy part of interactions between ECG parameters. (Summarized in Figure 42)

- There is a bidirectional GC link between ST elevation and RR interval
- ST-elevation granger causes the height of the R wave, but in converse the number of significant links is comparatively less.
- There is a bidirectional GC link between RR interval and R wave height.
- QRS duration sparsely connects with other parameters.

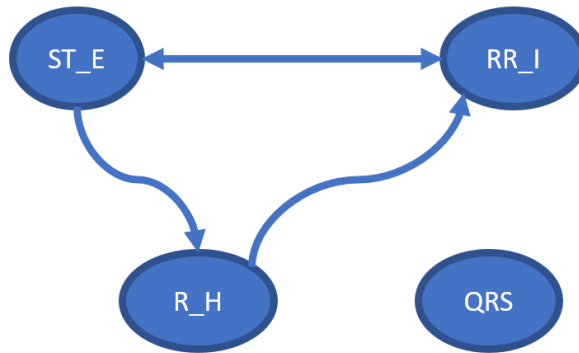


Figure 42: Significant links within ECG parameters are summarized in the graph. Where R\_h: R wave height , ST\_E : ST segment elevation, RR\_I : RR interval and QRS : QRS complex duration

Furthermore, most animals have the following similar properties common in their healthy part of interactions between respiration parameters. (Summarized in Figure 43)

- There are fewer significant links between the Peak expiratory flow and peak inspiratory flow.
- There are fewer significant links between the total volume and peak inspiratory flow.
- There is a bidirectional Granger causality link between the durations inspiration and expiration.
- Expiration duration granger causes the Peak expiratory flow, but in the reverse direction the number of significant links is comparatively less.
- Peak expiratory flow granger causes the total volume but in the reverse direction number of significant links is comparatively less.
- Expiration duration granger causes the total volume. In opposite way, the number of significant links is comparatively less.
- Inspiration time is sparsely affects peak inspiratory, expiratory flow and total volumne.
- Inspiration time is affected majorly by past peak expiratory flow as compared to past peak inspiratory flow.
- There are very less significant links between expiration time and peak inspiratory flow.

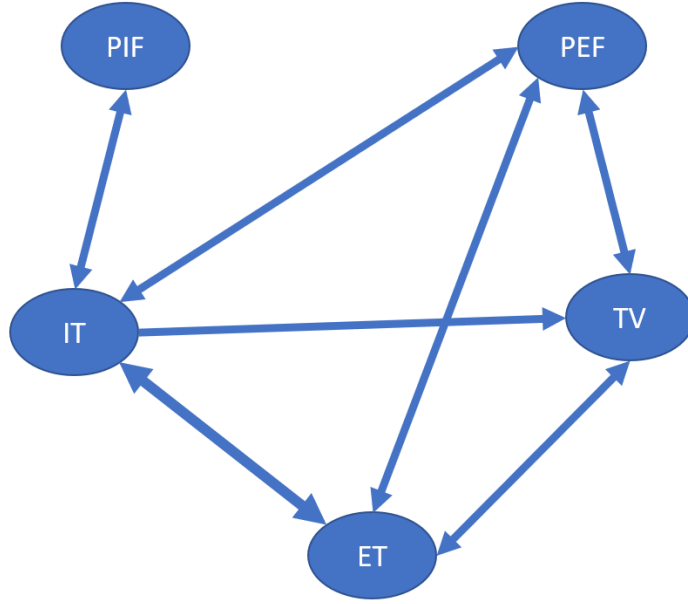


Figure 43: Significant links within breathing parameters are summarized in the graph. Where PIF: Peak Inspiratory flow, PEF: Peak expiratory flow, TV: Total Volume , ET: Expiration time, IT: Inspiration time and TV: Total volume

Moreover, no significant links were found out between the ECG and breathing parameters. This could be because, before calculating Granger relationships, we did the baseline correction to make the signal approximately stationary. Baseline correction removes the trend in the signal. These discarded trends might be because of interactions between ECG and breathing parameters.

Above step won't hamper the calculation of GCs if we analyse the signal over the short windows (around 600 samples). We have considered the 2000 samples size window of ECG while calculating the interactions between ECG and breathing parameters. If we reduce the window size of ECG, then the corresponding number of respiration samples will become less and this subsequently could cause the non-stationary problem while evaluating GCs. Therefore, we should employ such methods that can effectively investigate the interactions between two non-stationary signals.

The Figure 44 compares the box plot of mean weighted interaction graph density of breathing parameters (top row) and ECG parameters (bottom row) between healthy and exposed regions. Further, the left and the right columns plots illustrate the box plots of Fentanyl and VX chemicals, respectively. Where the top and bottom marks of each box plot indicate 75th and 25th percentile, respectively, and the middle edge represents the median value of the mean graph density. Finally, the whiskers in each box plot indicate extreme points that are not considered as outliers, and the outliers are indicated by star sign [62].

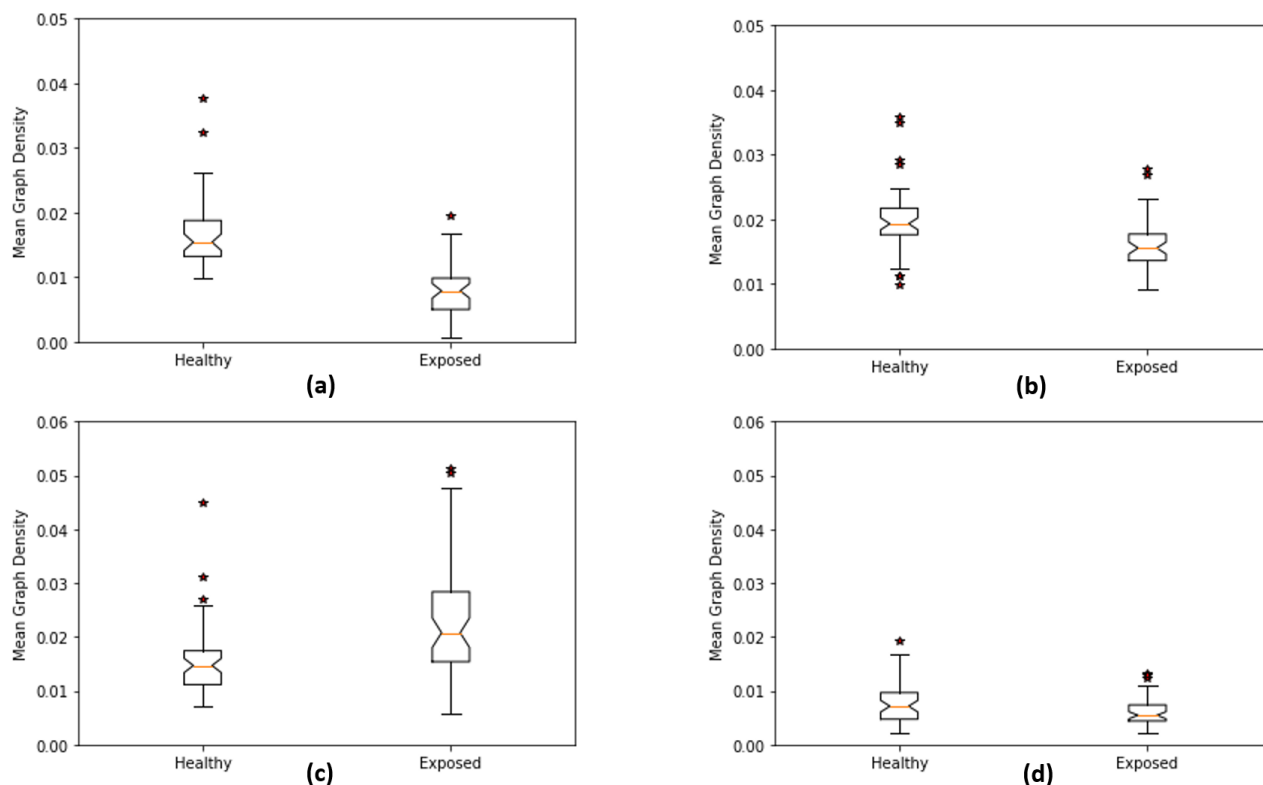


Figure 44: Comparison of Box plots of mean graph density(MGD). a) MGD of breathing interactions of Fentanyl b) MGD of breathing interactions of VX c) MGD of ECG interactions of Fentanyl d) MGD of ECG interactions of VX. There is a significant drop of MGD of breathing interactions as compared to ECG interactions after the exposure. The decrease is more prominent in the case of the Fentanyl chemical than the VX chemical.

According to the Figure 44, there is a significant drop in the mean graph density of breathing interactions after the exposure as compared to the mean graph density of ECG interactions. Further, the decrease is more significant in the case of the Fentanyl chemical than the VX chemical. This depicts that the granger causalities could be good features to differentiate between healthy and exposure.

Intravenous and subcutaneous are two different types of exposure of fentanyl chemical class, with varying dosages. The Figure 45, compares the distribution of mean graph density of breathing interactions between the low and high dosages of Fentanyl intravenous exposure (top row), and between the low and high dosages of Fentanyl subcutaneous exposure (bottom row).

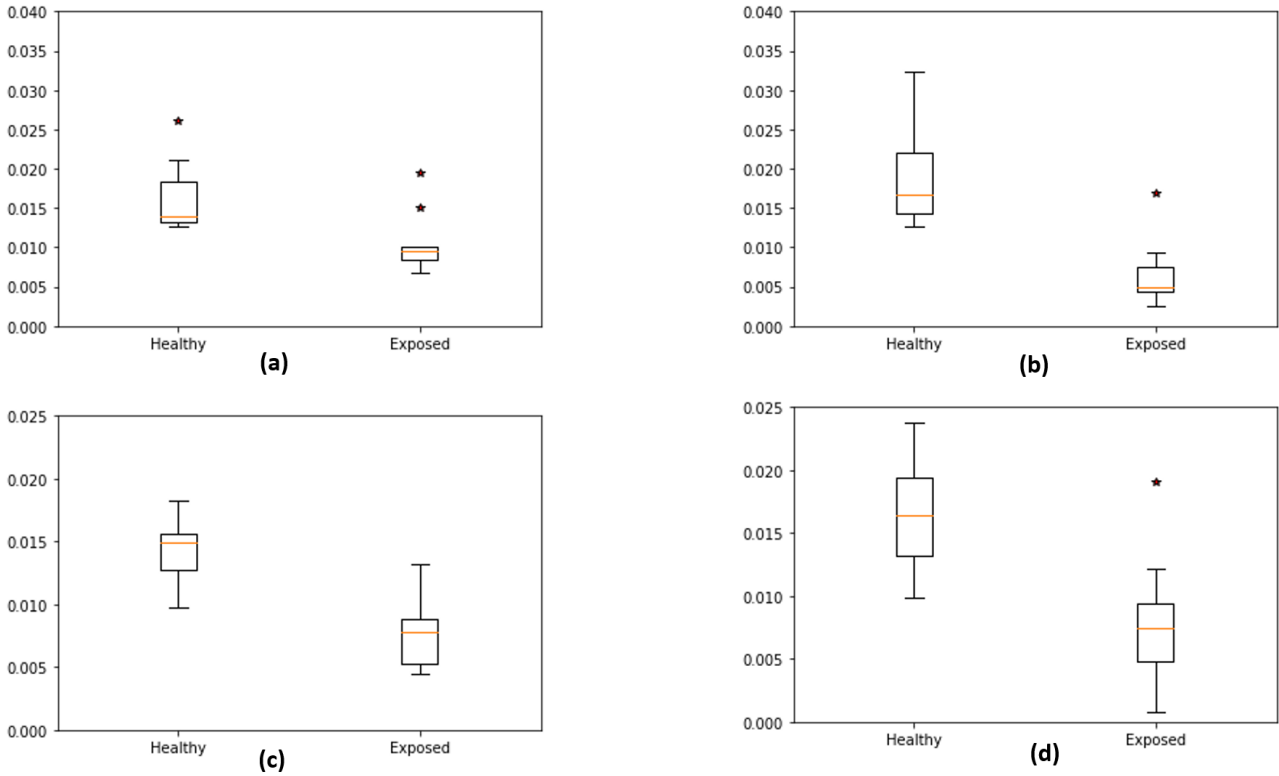


Figure 45: Comparison of Box plots of mean graph density(MGD). a) MGD of breathing interactions of Fentanyl Intravenous low dosage exposure b) MGD of breathing interactions of Fentanyl Intravenous high dosage exposure c) MGD of breathing interactions of Fentanyl Subcutaneous low dosage exposure d) MGD of breathing interactions of Fentanyl Subcutaneous high dosage exposure. For both intravenous and subcutaneous types of exposure, a higher dosage has more drops than the lower dosage quantity.

According to the Figure 45, there is a slightly more drop in the mean graph density of breathing interactions after the exposure for high dosage, for both types of Fentanyl exposure.

Further, the Figure 46, compares the distribution of mean graph density of ECG interactions between the low and high dosage of Fentanyl intravenous exposure (top row), and between the low and high dosage of Fentanyl subcutaneous exposure (bottom row).

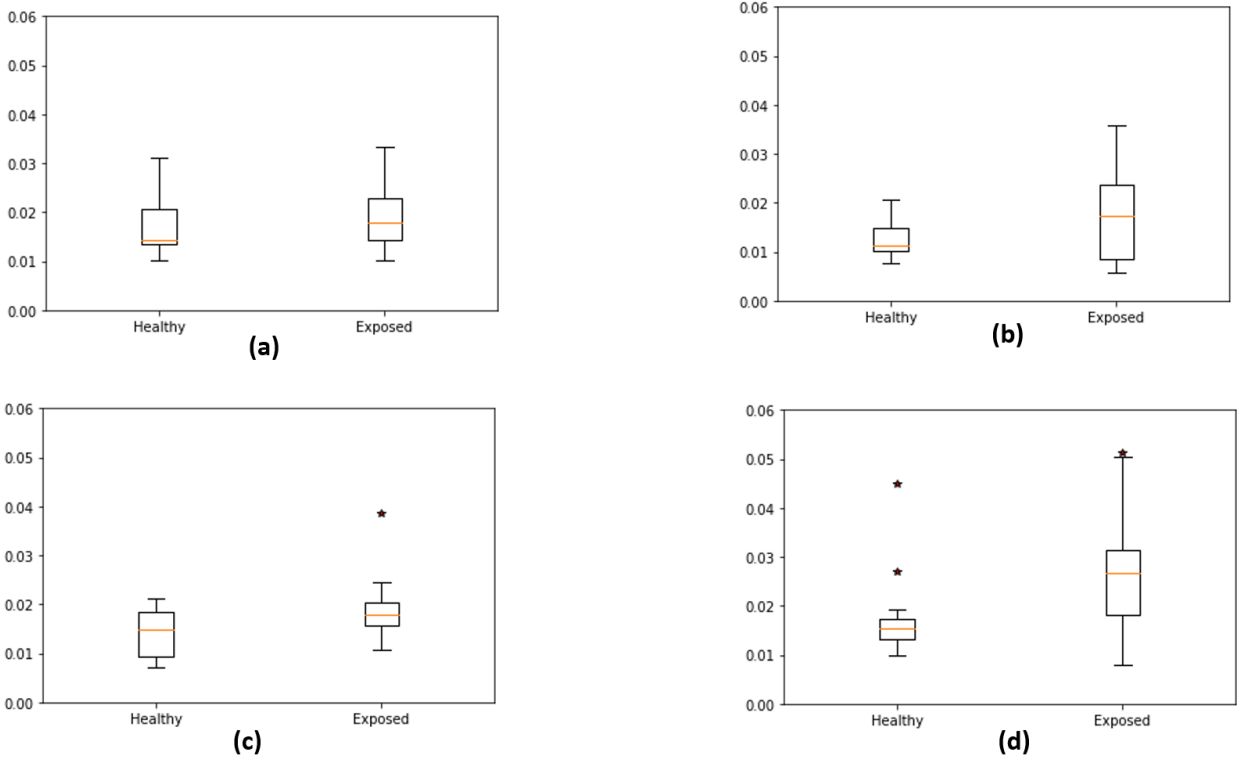


Figure 46: Comparison of Box plots of mean graph density(MGD). a) MGD of ECG interactions of Fentanyl Intravenous low dosage exposure b) MGD of ECG interactions of Fentanyl Intravenous high dosage exposure c) MGD of ECG interactions of Fentanyl Subcutaneous low dosage exposure d) MGD of ECG interactions of Fentanyl Subcutaneous high dosage exposure. For both intravenous(top row) and subcutaneous(bottom row) types of exposure, there is a slight increase in the strength of ECG interactions.

According to the Figure 46, there is a slight increase in the mean graph density of ECG interactions after the exposure fo both high and low dosages, for both types of Fentanyl exposure.

## 5.2 Classification Results

### 5.2.1 Evaluation Metrics

We used a confusion matrix to evaluate the performance of the classification models. A confusion matrix is an  $P * P$  matrix, where  $p$  is the number of classes. The matrix compares the true target labels with those of the predicted labels by the model. This metric is useful when the classes are unbalanced. According to the problem need, we could calculate the F-1 score, recall, precision, and accuracy from the confusion matrix [36]. In this project, we used the confusion matrix of size  $2 * 2$  and  $3 * 3$ .

Lets consider  $2*2$  confusion matrix as shown in Figure 47. Where

- T0 : It denotes all the data that belong to class-0 and are predicted as class-0
- TI : It denotes all the data that belong to class-1 and are predicted as class-1
- F0 : It denotes all the data that belong to class-1 and are predicted as class-0
- F1 : It denotes all the data that belong to class-0 and are predicted as class-1

Confusion Matrix		Predicted Label	
		Class 0	Class 1
True Label	Class 0	<b>T0</b>	<b>F1</b>
	Class 1	<b>F0</b>	<b>T1</b>

Figure 47: Confusion Matrix with two classes.

The four evaluation metrics that are used to access the model performance are accuracy, recall, precision and F-1 score. That are,

- Accuracy is the proportion of all the correctly classified instances of the whole dataset (equation (56)).
- Recall quantifies how well a model can classify a particular class correctly of all the available instances of that class. We calculated recall with respect to class-1 (equation (57)).
- Precision evaluates how many predicted particular class is a true class. We calculate precision with respect to class-1 (equation (58)).

We calculated the accuracy, recall and precision as

$$\text{Accuracy} = \frac{T0 + T1}{T0 + T1 + F0 + F1}, \quad (56)$$

$$\text{Recall} = \frac{T1}{T1 + F0}, \text{ and} \quad (57)$$

$$\text{Precision} = \frac{T1}{T1 + F1}, \text{ respectively.} \quad (58)$$

We considered class-0 and class-1 as healthy and exposed instances, respectively.

Similarly for three class confusion matrix ( Figure 48) we calculated accuracy, precision and recall as denoted in equations (59), (60) and (61), respectively. For example, 2F0 denotes all the data that belong to class-2 and are falsely predicted as class-0 and similarly, 0F1 denotes all the data that belong to class-0 and are falsely predicted as class-1.

Confusion Matrix		Predicted Label		
		Class 0	Class 1	Class 2
True Label	Class 0	<b>T0</b>	<b>0F1</b>	<b>0F2</b>
	Class 1	<b>1F0</b>	<b>T1</b>	<b>1F2</b>
	Class 2	<b>2F0</b>	<b>2F1</b>	<b>T2</b>

Figure 48: Confusion Matrix with three classes.

We calculated the accuracy, recall and precision for three class confusion matrix as

$$\text{Accuracy} = \frac{T0 + T1 + T2}{T0 + T1 + T2 + 1F0 + 2F0 + 0F1 + 2F1 + 0F2 + 1F2}, \quad (59)$$

$$\text{Precision (Class1)} = \frac{T1}{T2 + 0F1 + 2F0} \quad (60)$$

$$\text{Precision (Class2)} = \frac{T2}{T2 + 0F2 + 1F2}, \text{ and}$$

$$\begin{aligned} \text{Recall (Class1)} &= \frac{T1}{T2 + 1F0 + 1F2} \\ \text{Recall (Class2)} &= \frac{T2}{T2 + 2F0 + 2F1}, \text{ respectively.} \end{aligned} \tag{61}$$

We considered class-0, class-1 and class-3 as healthy instances, instances that are exposed via VX and instances that are exposed via Fentanyl, respectively.

### 5.3 Classification Results

We worked on two types of model

- Type-1 : Model that differentiate between healthy and exposure samples
- Type-2 : Model that differentiate between healthy samples, samples that are exposed by VX and samples that are exposed by Fentanyl.

We trained the above two models separately on interactions features set from ECG parameters and breathing parameters, and tested both the models on their independent test set. We did not train our model on the feature set considering the interaction between ECG and breathing because there were no significant interaction between them.

Moreover, for each type of model, we evaluated sample by sample performance and animal by animal performance. Where animal by animal performance is evaluated by grouping the predicted samples and then according to maximum occurrence the animal by animal performance is evaluated.

The classification results of 2 way classification model (sample by sample) is shown in Figure 49. Where

- Vx (Recall) : Indicates the percentage of the exposure samples due to VX chemical that were detected correctly.
- Fentanyl (Recall) : Indicates the percentage of the exposure samples due to Fentanyl chemical that were detected correctly.
- VX (Recall) Healthy : Indicates the percentage of the healthy samples in VX chemical class that were detected correctly as healthy.
- Fentanyl (Recall) Healthy : Indicates the percentage of the healthy samples in Fentanyl chemical class that were detected correctly as healthy.

	Breathing Parameters		ECG Parameters	
	Random Forest	SVM	Random Forest	SVM
<b>Accuracy</b>	75.43	78.04	66.89	65.15
<b>Recall</b>	67.54	67.33	56.07	45.15
<b>Precision</b>	80.91	86.14	79.41	87.17
<b>F-1 Score</b>	73.62	75.69	65.73	59.45
<b>VX (Recall)</b>	57.51	57.34	40.25	26.27
<b>Fentanyl (Recall)</b>	81.19	80.95	71.08	62.97
<b>VX(Recall) Healthy</b>	86.29	91.87	77.31	90.81
<b>Fentanyl (Recall) Healthy</b>	81.69	87.14	83.52	91.69

Figure 49: The results of the 2 way classification model trained with SVM and random forest on breathing and ECG based parameters. The model based on breathing interactions is performing better than the ECG interactions. SVM trained on breathing interactions performs better than random forest. Whereas, random forest trained on ECG interactions performs better than the SVM.

According to the confusion matrix in Figure 49. The breathing interactions are more informative than ECG interactions in differentiating between the chemicals. The performance of SVM ( radial basis function) is better

than the random forest classifier. Further, the model is doing well in classifying Fentanyl exposure samples than the VX exposure samples because the Fentanyl (recall) is higher than VX (recall). Moreover, for the healthy region, the model performed equally well for both types of chemicals because VX(recall) healthy and Fentanyl ( recall) healthy are approximately equal.

The classification results of 2 way classification model (animal by animal) is shown in Figure 50. Where

- VX(Recall) is proportional to the correctly classified VX exposed animals from the total of VX exposed animals.
- Fentanyl(Recall) is proportional to the correctly classified VX exposed animals from the total of VX exposed animals.

	Breathing Parameters		ECG Parameters	
	Random Forest	SVM	Random Forest	SVM
Accuracy	85.71 (18/21)	85.71 (18/21)	50 (11/22)	45.45(10/22)
VX (Recall)	72.72 (8/11)	72.72 (8/11)	9.09 (1/11)	9.09 (1/11)
Fentanyl (Recall)	100 (10/10)	100 (10/10)	90.90 (10/11)	81.81(9/11)

Figure 50: The results of the 2 way classification model (animal by animal) trained with SVM and random forest by using breathing and ECG based parameters, separately. Model-based on breathing interactions performs better than the one with ECG interactions.

The model is able to classify healthy animals with 100% accuracy into healthy set. Whereas it correctly detected 18 out of 21 animals as exposure. The model is able to detect all the animals of fentanyl class but wrongly classified 3 animals of VX class as healthy. The confusion matrix of one case is shown in Figure 51. Since we have considered zero healthy instances therefore we omitted the precision and F-1 score from above figure.

SVM Breathing Parameter		Predicted Label	
Only Exposure part is taken		Healthy	Exposure
True Label	Healthy	0	0
	Exposure	3 =(3+0)	18=(8+10)

Figure 51: Confusion matrix of one of the above case.

The classification results of model 3 way classification model (sample by sample) are shown in Figure 52.

	Breathing Parameters		ECG Parameters	
	Random Forest	SVM	Random Forest	SVM
Accuracy	65.55	71.69	57.87	56.36
Recall (VX)	34.61	38.11	11.68	0.7
Precision(VX)	65.34	82.57	54.86	68
F-1 Score (VX)	45.25	69.04	19.26	1.4
Recall (Fentanyl)	49.76	69.04	59.12	49.49
Precision (Fentanyl)	67.85	75.52	68.22	71.22
F-1 Score (Fentanyl)	57.41	72.13	63.33	58.4

Figure 52: Results of 3 way classification model trained with SVM and random forest by using breathing or ECG based parameters.

In 3 way model we considered healthy, VX and Fentanyl as class 0 , class 1 and class 2, respectively. According to the above Figure, The breathing interactions are more informative than ECG interactions in differentiating

between the chemicals. The performance of SVM ( radial basis function) is better than the random forest classifier. Further, the model is doing well in classifying Fentanyl exposure samples than the VX exposure samples because the Fentanyl (recall) and F1 score, is higher than VX (recall) and F1 score, respectively. Moreover, for the healthy region, the model performing equally well for both types of chemicals because VX(recall) healthy and Fentanyl (recall) healthy are approximately equal.

The classification results of 3 way classification model (animal by animal) are shown in Figure 53.

	Breathing Parameters		ECG Parameters	
	Random Forest	SVM	Random Forest	SVM
Accuracy	6/21	12/21	3/22	5/22
Recall (VX)	1/11	2/11	0/11	0/11
Precision(VX)	-	-	-	-
Recall (Fentanyl)	5/10	9/10	3/11	5/11
Precision (Fentanyl)	-	-	-	-

Figure 53: The results of 3 way classification model trained with SVM and random forest on breathing and ECG based parameters. The model based on breathing interactions is performing better than the ECG interactions. SVM trained on breathing interactions performs better than random forest. Whereas, random forest trained on ECG interactions performs better than the SVM.

The SVM model with breathing parameters is able to classify healthy animals with 100% accuracy into healthy set. Whereas, it detected chemical correctly of 12 out of 21 animals. The model is able to detect 9 out of 10 animals of fentanyl class but only detects 2 out of 11 of VX class. The confusion matrix of SVM model is shown in Figure 54. Since we have considered zero healthy instances therefore we omitted the precision and F-1 score from above figure.

The confusion matrix of one case is shown in figure-54.

True Label	Predicted Label			
	Random Forest	Healthy	Fentanyl	VX
Healthy		0	4	10
Fentanyl		4	5	0
VX		10	1	1

Figure 54: Confusion matrix of one of the above case

## 6 Conclusion

### 6.1 Future Work

The immediate future work of this thesis would be of testing the algorithm on human datasets and mapping the results with those of Guinea pigs. This project concluded with a decent accuracy of 78% and 71% for model type-1 and type-2 respectively on the independent test set of Guinea pigs. But still, the performance of the model can be improved further.

First, we used principal component analysis (PCA) for feature transformation. The major drawback of PCA is that it is biased towards the animal that has highly variant Granger causality values. We intended to have a common subspace that maximizes the variance among the features almost equally for all the animals. To achieve this, we can use the technique of tensor decomposition [24]. We used PCA only on healthy samples because the nature of exposure samples are different due to the difference in injected dosage quantity. Linear discriminate analysis (LDA) and Quadratic discriminate analysis (QDA) [30] are supervised ways of features transformation. We can use LDA or QDA to find the subspace to get the highest variation between healthy and exposure samples for a better projection.

Secondly, the EEG power bands have proven to be useful in differentiating between the VX and Fentanyl [61]. In this thesis, we have not considered the EEG power bands because of their synchronization issue. Adding the EEG features into the coupling analysis can further enhance the classification accuracy and provide insightful learning of how the EEG power bands interact with ECG and breathing parameters.

Besides classification, we also concluded that we did not find any noticeable interactions between the ECG and breathing parameters. Here, we use the conditional Granger causality method to evaluate the interactions. In the future, we can investigate the heuristic method of granger causality between two parameters without considering the effect of others. Later, we can employ some source localization techniques on the interaction graph to find the prominent nodes that connect two networks, that is ECG and breathing interaction networks.

Before calculating Granger relationships, we did the baseline correction to make the signal approximately stationary. Baseline correction removes the trend in the signal. The discarded trends might be because of interactions between ECG and breathing parameters. Therefore in future, we should employ methods that can effectively investigate the interactions between two non-stationary signals.

Further, the proposed algorithm cannot detect the non-linear interactions between the signals. To overcome this, we can either introduce the radial basis kernel [26] in regression equations or solve the equations using the LSTMs [56]. Further, we can use different methods like the nearest neighbour [45] to calculate the non-linear couplings between the signals.

Based on the initial research, we figured out that the non-linear classification models (random forest and SVM with radial basis kernel) are performing well. So, implementing multi-layers perceptron (deep learning model) seems a promising choice for future work.

Finally, to get a whole new perspective on interactions between the physiological signals, we can work on raw signals of EEG, ECG and respiration signals. Here we can sample the respiration signal at the onset of R peak occurrence and simultaneously calculate the EEG power band values for the corresponding segments. Such an approach will cause the development of a more robust and adaptable classification algorithm from scratch.

## 6.2 Conclusion

The causal algorithm investigates the direction and strength of a variable to another variable of a system. We implemented a conditional granger causality that considers the effect of all the variables in the system while evaluating the coupling between any other two variables. We worked with the parameters of ECG and respiration signals. And explored how the interactions within the ECG parameters, respiration parameters, and between ECG and breathing change from healthy to exposure state.

The curse of dimensionality is one of the major problems of high dimensional conditional granger causality. We introduced the cardinality constraint in the loss function and showed that the new optimized algorithm can detect all the links with a small sample size. To avoid false causalities, we used F-test and surrogate analysis.

After evaluating the coupling values, we did some exploratory analysis on them. We found out that there is a significant drop in mean graph density of breathing interactions after the exposure, and the decrease was more significant in the Fentanyl's class of chemical. But, in the case of the mean graph density of ECG interactions, we observed no noticeable change. Furthermore, no significant links are found to be there between the ECG and breathing parameters.

Then, we develop two types of classification models (exposure vs healthy and healthy vs VX vs Fentanyl). We first standardized the coupling values separately for each of the animals with respect to their healthy coupling values. After standardization, we transformed the features to a new rotated space that accounts for most variations in the healthy casualties' values. Based on the initial research, we figured out that the non-linear classification models (random forest and SVM with radial basis kernel) performed well. We then implemented features forward selection and hyper-parameter tuning using a cross-validation approach.

We tested the final optimized model on an independent test set. The SVM model with breathing parameters achieved the highest accuracy in both types of models. Further, the performance of the model is much better for the fentanyl chemical than the VX chemical. Finally, we highlighted some drawbacks in the current implementation and unanswered questions that pave the way for future work.

## References

- [1] R Bellman. “Dynamic programming princeton university press princeton”. In: *New Jersey Google Scholar* (1957).
- [2] Raymond B Cattell. “The scree test for the number of factors”. In: *Multivariate behavioral research* 1.2 (1966), pp. 245–276.
- [3] Clive WJ Granger. “Investigating causal relations by econometric models and cross-spectral methods”. In: *Econometrica: journal of the Econometric Society* (1969), pp. 424–438.
- [4] Gideon Schwarz. “Estimating the dimension of a model”. In: *The annals of statistics* (1978), pp. 461–464.
- [5] TJ Ulrych and M Ooe. “Autoregressive and mixed autoregressive-moving average models and spectra”. In: *Nonlinear Methods of Spectral Analysis* (1979), pp. 73–125.
- [6] Hamparsum Bozdogan. “Model selection and Akaike’s information criterion (AIC): The general theory and its analytical extensions”. In: *Psychometrika* 52.3 (1987), pp. 345–370.
- [7] Thomas Chang-Yao Tsao et al. “Respiratory failure of acute organophosphate and carbamate poisoning”. In: *Chest* 98.3 (1990), pp. 631–636.
- [8] JE Bright et al. “A histochemical study of changes observed in the mouse diaphragm after organophosphate poisoning”. In: *Human & experimental toxicology* 10.1 (1991), pp. 9–14.
- [9] Belur V Dasarathy. “Nearest neighbor (NN) norms: NN pattern classification techniques”. In: *IEEE Computer Society Tutorial* (1991).
- [10] James Theiler et al. “Testing for nonlinearity in time series: the method of surrogate data”. In: *Physica D: Nonlinear Phenomena* 58.1-4 (1992), pp. 77–94.
- [11] H Nozaki et al. “A case of VX poisoning and the difference from sarin”. In: *The Lancet* 346.8976 (1995), pp. 698–699.
- [12] Ian RH Falloon et al. “Early detection and intervention for initial episodes of schizophrenia”. In: *Schizophrenia Bulletin* 22.2 (1996), pp. 271–282.
- [13] Sky McKinley and Megan Levine. “Cubic spline interpolation”. In: *College of the Redwoods* 45.1 (1998), pp. 1049–1060.
- [14] Thomas M Cover. *Elements of information theory*. John Wiley & Sons, 1999.
- [15] John Platt et al. “Probabilistic outputs for support vector machines and comparisons to regularized likelihood methods”. In: *Advances in large margin classifiers* 10.3 (1999), pp. 61–74.
- [16] Thomas Schreiber. “Measuring information transfer”. In: *Physical review letters* 85.2 (2000), p. 461.
- [17] Thomas Schreiber and Andreas Schmitz. “Surrogate time series”. In: *Physica D: Nonlinear Phenomena* 142.3-4 (2000), pp. 346–382.
- [18] Leo Breiman. “Random forests”. In: *Machine learning* 45.1 (2001), pp. 5–32.
- [19] Jerome Friedman, Trevor Hastie, Robert Tibshirani, et al. *The elements of statistical learning*. Vol. 1. 10. Springer series in statistics New York, 2001.
- [20] Bradley Efron et al. “Least angle regression”. In: *The Annals of statistics* 32.2 (2004), pp. 407–499.
- [21] Harry Zhang. “The optimality of naive Bayes”. In: *AA* 1.2 (2004), p. 3.
- [22] Ian Jolliffe. “Principal component analysis”. In: *Encyclopedia of statistics in behavioral science* (2005).
- [23] Dieter Jungnickel and D Jungnickel. *Graphs, networks and algorithms*. Springer, 2005.
- [24] Brett W. Bader and Tamara G. Kolda. “Algorithm 862: MATLAB Tensor Classes for Fast Algorithm Prototyping”. In: *ACM Trans. Math. Softw.* 32.4 (Dec. 2006), pp. 635–653. ISSN: 0098-3500. DOI: [10.1145/1186785.1186794](https://doi.org/10.1145/1186785.1186794). URL: <https://doi.org/10.1145/1186785.1186794>.
- [25] Ahmet Cosar and Levent Kenar. “An anesthesiological approach to nerve agent victims”. In: *Military medicine* 171.1 (2006), pp. 7–11.
- [26] Daniele Marinazzo, Mario Pellicoro, and Sebastiano Stramaglia. “Nonlinear parametric model for Granger causality of time series”. In: *Physical Review E* 73.6 (2006), p. 066216.
- [27] Katerina Hlaváčková-Schindler et al. “Causality detection based on information-theoretic approaches in time series analysis”. In: *Physics Reports* 441.1 (2007), pp. 1–46.
- [28] Milan Paluš and Martin Vejmelka. “Directionality of coupling from bivariate time series: How to avoid false causalities and missed connections”. In: *Physical Review E* 75.5 (2007), p. 056211.
- [29] Luca Faes, Alberto Porta, and Giandomenico Nollo. “Mutual nonlinear prediction as a tool to evaluate coupling strength and directionality in bivariate time series: Comparison among different strategies based on  $k$  nearest neighbors”. In: *Phys. Rev. E* 78 (2 Aug. 2008), p. 026201. DOI: [10.1103/PhysRevE.78.026201](https://doi.org/10.1103/PhysRevE.78.026201). URL: <https://link.aps.org/doi/10.1103/PhysRevE.78.026201>.
- [30] Trevor Hastie, Robert Tibshirani, and Friedman, J. (2009): *The elements of statistical learning. Data mining, inference, and prediction*. 2008.
- [31] Thomas Maiwald et al. “Surrogate data—A qualitative and quantitative analysis”. In: *Mathematical Methods in Signal Processing and Digital Image Analysis*. Springer, 2008, pp. 41–74.

- [32] Lionel Barnett, Adam B Barrett, and Anil K Seth. “Granger causality and transfer entropy are equivalent for Gaussian variables”. In: *Physical review letters* 103.23 (2009), p. 238701.
- [33] Gopikrishna Deshpande et al. “Multivariate Granger causality analysis of fMRI data”. In: *Human brain mapping* 30.4 (2009), pp. 1361–1373.
- [34] Richard E Frye and Meng-Hung Wu. “Multichannel least-squares linear regression provides a fast, accurate, unbiased and robust estimation of Granger causality for neurophysiological data”. In: *Computers in biology and medicine* 41.12 (2011), pp. 1118–1131.
- [35] Javier Martín Hernández and Piet Van Mieghem. “Classification of graph metrics”. In: *Delft University of Technology: Mekeweg, The Netherlands* (2011), pp. 1–20.
- [36] Yuichiro Anzai. *Pattern recognition and machine learning*. Elsevier, 2012.
- [37] Bojan Musizza et al. “Fluctuations and interactions between brain waves during deep and shallow anesthesia”. In: *Fluctuation and Noise Letters* (2012).
- [38] Yuri Shiogai et al. “Cortico-cardio-respiratory network interactions during anesthesia”. In: (2012).
- [39] Lars Buitinck et al. “API design for machine learning software: experiences from the scikit-learn project”. In: *ECML PKDD Workshop: Languages for Data Mining and Machine Learning*. 2013, pp. 108–122.
- [40] James Gareth et al. *An introduction to statistical learning: with applications in R*. Springer, 2013.
- [41] Christophe Leys et al. “Detecting outliers: Do not use standard deviation around the mean, use absolute deviation around the median”. In: *Journal of experimental social psychology* 49.4 (2013), pp. 764–766.
- [42] Steffen Schulz et al. “Cardiovascular and cardiorespiratory coupling analyses: a review”. In: *Philosophical Transactions of the Royal Society A: Mathematical, Physical and Engineering Sciences* 371.1997 (2013), p. 20120191.
- [43] Philippe Arlotto et al. “An ultrasonic contactless sensor for breathing monitoring”. In: *Sensors* 14.8 (2014), pp. 15371–15386.
- [44] Jia Li and Ridge Regression Linear. “Principal component analysis”. In: *Multivariate Statistics; Springer: Berlin, Germany* 487 (2014), pp. 163–183.
- [45] Alessandro Montalto, Luca Faes, and Daniele Marinazzo. “MuTE: a MATLAB toolbox to compare established and novel estimators of the multivariate transfer entropy”. In: *PloS one* 9.10 (2014), e109462.
- [46] Luca Faes et al. “Linear and non-linear brain–heart and brain–brain interactions during sleep”. In: *Physiological measurement* 36.4 (2015), p. 683.
- [47] A Kuo et al. “In vivo profiling of seven common opioids for antinociception, constipation and respiratory depression: no two opioids have the same profile”. In: *British journal of pharmacology* 172.2 (2015), pp. 532–548.
- [48] Rangaraj M Rangayyan. *Biomedical signal analysis*. John Wiley & Sons, 2015.
- [49] Donna Barto. “Recognizing ST-segment elevation”. In: *Nursing2020 Critical Care* 11.2 (2016), pp. 5–6.
- [50] Mohssen Mohammed, Muhammad Badruddin Khan, and Eihab Bashier Mohammed Bashier. *Machine learning: algorithms and applications*. Crc Press, 2016.
- [51] Andreas Müller et al. “Causality in physiological signals”. In: *Physiological measurement* 37.5 (2016), R46.
- [52] Zitong Zhang et al. “Choosing wavelet methods, filters, and lengths for functional brain network construction”. In: *PloS one* 11.6 (2016), e0157243.
- [53] Michal Javorka et al. “Causal analysis of short-term cardiovascular variability: state-dependent contribution of feedback and feedforward mechanisms”. In: *Medical & biological engineering & computing* 55.2 (2017), pp. 179–190.
- [54] Beth Jelfs and Rosa HM Chan. “Directionality indices: Testing information transfer with surrogate correction”. In: *Physical Review E* 96.5 (2017), p. 052220.
- [55] Sara Magliacane et al. “Domain adaptation by using causal inference to predict invariant conditional distributions”. In: *arXiv preprint arXiv:1707.06422* (2017).
- [56] Aneesh Sreevallabh Chivukula, Jun Li, and Wei Liu. “Discovering granger-causal features from deep learning networks”. In: *Australasian Joint Conference on Artificial Intelligence*. Springer. 2018, pp. 692–705.
- [57] Mohamed Hammad et al. “Detection of abnormal heart conditions based on characteristics of ECG signals”. In: *Measurement* 125 (2018), pp. 634–644.
- [58] Will Koehrsen. “Overfitting vs. underfitting: A complete example”. In: *Towards Data Science* (2018).
- [59] Nikola N Radovanović et al. “Bidirectional cardio-respiratory interactions in heart failure”. In: *Frontiers in physiology* 9 (2018), p. 165.
- [60] Piet Van Mieghem. “Directed graphs and mysterious complex eigenvalues”. In: *Google Scholar* (2018).
- [61] Jan Ubbo van Baardewijk et al. “Early detection of exposure to toxic chemicals using continuously recorded multi-sensor physiology”. In: *Sensors* 21.11 (2021), p. 3616.

- [62] Matplotlib. *Box Plot*. [http://https://matplotlib.org/3.1.1/api/\\_as\\_gen/matplotlib.pyplot.boxplot.html](http://https://matplotlib.org/3.1.1/api/_as_gen/matplotlib.pyplot.boxplot.html).
- [63] Matlab. *Introduction to Wavelet Families*. <https://nl.mathworks.com/help/wavelet/gs/introduction-to-the-wavelet-families.html#f3-1008627>.
- [64] Matlab. *maximum overlap discrete wavelet transform*. <https://nl.mathworks.com/help/wavelet/ref/modwt.html>.
- [65] Wikipedia. *Spearman's rank correlation coefficient*. [https://en.wikipedia.org/wiki/Spearman%27s\\_rank\\_correlation\\_coefficient](https://en.wikipedia.org/wiki/Spearman%27s_rank_correlation_coefficient).
- [66] wikipedia. *Encyclopedia of Mathematics*. [http://encyclopediaofmath.org/index.php?title=Spline\\_interpolation&oldid=48784](http://encyclopediaofmath.org/index.php?title=Spline_interpolation&oldid=48784).
- [67] wikipedia. *Median absolute deviation*. [https://en.wikipedia.org/wiki/Median\\_absolute\\_deviation](https://en.wikipedia.org/wiki/Median_absolute_deviation).